ANALYTICAL REPRESENTATIONS OF FLUID-STRUCTURE INTERACTION NOISE FOR LARGE EDDY SIMULATIONS

M. S. Howe
Boston University, College of Engineering
110 Cummington Street, Boston MA 02215
27 March, 2000

Report AM-00-003

Final Report
Prepared for Dr. L. Patrick Purtell
Office of Naval Research, Code 333
Grant N00014-99-1-0391

CONTENTS

CHAPTER 1

EDGE-SOURCE ACOUSTIC GREEN'S FUNCTION FOR AN AIRFOIL OF ARBITRARY CHORD

SUMMARY

Approximations are derived for the three-dimensional, time-harmonic acoustic Green's function whose normal derivative vanishes on the surface of an airfoil of finite thickness and chord ℓ for source locations in the neighborhood of either the leading or trailing edge. The acoustic wavelength is assumed to be large relative to the airfoil thickness, but no restriction is placed on its magnitude relative to ℓ. A multiple scattering calculation is performed for high frequencies that involves the successive scattering of waves from the leading and trailing edges of the airfoil. The 'principal subseries' of the expansion is summed and shown to provide an excellent approximation for the Green's function when $\kappa_o \ell \geq 1$, where κ_o is the acoustic wavenumber. The solution is extended down to $\kappa_o \ell = 0$ by interpolation with the corresponding Green's function for an airfoil of acoustically compact chord. The results extend the single scattering approximation introduced by Amiet [1], and are illustrated by application to the problem of trailing edge noise generated by nominally steady, low Mach number flow past the airfoil. Experiments and numerical simulations of such flows often include acoustic frequencies that are sufficiently small that the usual assumption of trailing-edge noise theory, that the airfoil is semi-infinite, is not valid.

1.1 INTRODUCTION

The 'self noise' produced by nominally steady, high Reynolds number flow over the trailing edge of an airfoil is usually attributed to the 'diffraction' of turbulence velocity fluctuations by the edge [2 - 13]. The turbulence is generated within the unstable boundary layer approaching the edge and is swept past the edge by the mean flow. The typical eddy dimension is usually small, being of the order of the boundary layer thickness. The sound therefore tends to be of relatively high frequency, with amplitude and spectral characteristics dependent on both the geometry of the airfoil trailing edge and on the details of flow separation at the edge [9 - 11, 14 - 16].

Most estimates of trailing edge noise have involved the assumption that the frequency is sufficiently large that the acoustic wavelength may be regarded as very much smaller than the airfoil chord. Diffraction theory predictions were therefore made by replacing the airfoil by a semi-infinite, rigid plane [2 - 6]. Adamczyk [17], Amiet [18, 19] and Martinez & Widnall [20] have studied theoretically the sound produced by turbulence and discrete gusts incident on a thin plate airfoil, including a 'single scattering' correction to allow for the influence of *finite* chord; the unsteady lift was first calculated and the radiation subsequently determined by means of Curle's [21] surface integral representation of aerodynamic sound. A similar procedure [22, 23] has been proposed for including the influence of finite chord on trailing edge noise. Such corrections are usually believed to be small at the high frequencies spanned by the edge noise spectrum. However, this may not be universally true at the very low Mach numbers encountered in underwater applications. In such cases it is often required to be able to predict the edge noise from data derived from turbulence wall pressure measurements near the edge or from numerical simulation of the edge flow [15, 16]. This data will essentially describe the hydrodynamic (incompressible) properties of the motion near the edge, and cannot be used to predict the radiation using Curle's formula, because the latter requires accurate phase information of the surface pressure *in the acoustic domain* when the surface is not acoustically compact [15].

This conclusion has important implications for the validation of trailing edge noise predictions obtained by numerical simulations at low Mach numbers. Current numerical algorithms are restricted to relatively low Reynolds numbers, for which the edge noise spectrum extends down to frequencies where the acoustic wavelength is comparable to the airfoil chord. Similarly, the airfoil thickness near the trailing edge is often too large to permit the acoustic radiation to be estimated with confidence from thin airfoil theory [8 - 11,

24 - 26]. Separation near the edge can lead to the production of large scale flow structures that generate significant acoustic energy at low frequencies. In these circumstances a proper comparison with experiment of predictions of the sound from the numerical simulations can be made only when both the finite chord and finite thickness of the airfoil are properly incorporated into the aeroacoustic theory. That is the subject of this chapter.

The radiated sound can be calculated in terms of the hydrodynamic edge flow and a suitable Green's function G [14]. In the following attention is confined to a rigid airfoil, for which Green's function is required to have vanishing normal derivative on the airfoil surface. The mean flow Mach number is assumed to be very small (appropriate to underwater applications) so that the acoustic wavelength may always be regarded as large compared to the airfoil *thickness.* An approximate representation of G will be derived in two steps. First the airfoil chord is assumed to exceed the characteristic wavelength of the sound, and the corresponding approximation for G is obtained by considering a multiple-scattering problem in which sound waves are successively scattered from the leading and trailing edges of the airfoil. This generalizes Amiet's [1] single scattering approximation, and incorporates, in addition, the influence of the finite thickness of the edge; it is also more convenient than Amiet's original formulation because it does not require an explicit evaluation of the unsteady lift distribution, nor does it require the aeroacoustic (turbulence) sources to be convecting in a prescribed manner. Second, this high frequency approximation is used in conjunction with Green's function for an airfoil with an *acoustically compact* chord to derive an interpolated, composite Green's function that is expected to be valid for all frequencies.

The relevant integral representations of trailing edge noise at low Mach numbers are recalled in §2, and the generalized Green's function is derived in §3. Application is made in §4 to determine the influence of finite chord on traditional predictions of trailing edge noise

1.2. REPRESENTATION OF THE EDGE NOISE

Consider the sound generated by low Mach number, turbulent flow of a homogeneous fluid of mean density ρ_o and sound speed c_o in the vicinity of the trailing edge of a rigid, two-dimensional airfoil. The discussion will be framed in terms of the canonical, parallel-sided airfoil shape illustrated schematically in Figure 1, which has chord ℓ and uniform thickness h, and a rounded nose. Blake and his coworkers [8 - 11] have made extensive measurements of the edge flow and sound produced by airfoils of this type with a variety of rounded, 'knuckled' and beveled trailing edges. Low Mach number turbulent flow past this airfoil type is also the subject of numerical simulations by Wang [24 - 26].

Introduce the rectangular coordinate system (x_1, x_2, x_3) with origin O at a convenient point near the trailing edge such that the 'upper' and 'lower' planar surfaces of the airfoil are at $x_2 = \pm\frac{1}{2}h$, the x_1-axis is in the direction of the mean flow, and x_3 is parallel to the airfoil span (out of the plane of the paper in Figure 1a). The mean flow velocity outside the boundary layers on the airfoil is assumed to be at sufficiently low subsonic speed U (in the positive x_1-direction) that the convection of sound may be neglected. This will be the case provided the Mach number $M = U/c_o \ll 1$; this condition also ensures that ρ_o and c_o may be regarded as constant throughout the flow.

When these conditions are satisfied the far field acoustic pressure fluctuations $p(\mathbf{x},\omega)e^{-i\omega t}$ of frequency ω produced by the interaction of the turbulence with the airfoil can be expressed in the form [14, 15]

$$\frac{p(\mathbf{x},\omega)}{\rho_o} = \int \frac{\partial G}{\partial \mathbf{y}}(\mathbf{x},\mathbf{y},\omega)\cdot\big(\boldsymbol{\Omega}\wedge\mathbf{v}\big)(\mathbf{y},\omega)d^3\mathbf{y} - \nu\oint_S \boldsymbol{\Omega}(\mathbf{y},\omega)\wedge\frac{\partial G}{\partial \mathbf{y}}(\mathbf{x},\mathbf{y},\omega)\cdot\mathbf{n}\,dS(\mathbf{y}), \quad (1)$$

where $\mathbf{v}$ is the fluid velocity, $\boldsymbol{\Omega} = \operatorname{curl}\mathbf{v}$ is the vorticity, and ν is the kinematic coefficient of shear viscosity. The second integral is taken over the surface S of the airfoil (with surface element $\mathbf{n}dS(\mathbf{y})$, and with the unit normal $\mathbf{n}$ directed *into* the fluid), and represents the contribution to the radiation from the unsteady skin friction; it can usually be ignored when the Reynolds number is large. The function $G(\mathbf{x},\mathbf{y},\omega)$ is the *time harmonic* Green's function. This has *outgoing* wave-behavior, vanishing normal derivative $\partial G(\mathbf{x},\mathbf{y};\omega)/\partial y_n = 0$ on S, and satisfies

$$(\nabla^2 + \kappa_o^2)G = \delta(\mathbf{x}-\mathbf{y}), \quad (2)$$

where $\kappa_o = \omega/c_o$ is the acoustic wavenumber.

Equation (1) is strictly valid when the flow is homentropic [27], when the pressure p can be regarded as a function of the density ρ. It can be used to calculate the sound radiated

from unsteady (vortical) regions provided the source terms $\big(\mathbf{\Omega} \wedge \mathbf{v}\big)(\mathbf{y},\omega)$ and $\mathbf{\Omega}(\mathbf{y},\omega)$ are known, either from measurement or from a preliminary numerical simulation of the flow. The notation here implies that a source term $F(\mathbf{y},t)$, say, is known as a function of source position $\mathbf{y}$ and of the time t, and that $F(\mathbf{y},\omega) = \frac{1}{2\pi}\int_{-\infty}^{\infty} F(\mathbf{y},t)\mathrm{e}^{i\omega t}dt$ is the Fourier transform with respect to the time.

The contribution from the volume integral in equation (1) can be recast at very low Mach numbers as a surface integral over S involving the 'upwash' velocity induced on S by the turbulence [15]. This representation for the particular case of an airfoil of zero thickness ($h = 0$) corresponds to the original diffraction theory of trailing edge noise developed by Chase [3, 5] and Chandiramani [4], which can also be expressed in the form

$$\begin{aligned} p(\mathbf{x},\omega) &= -\oint_{\mathrm{S}} G(\mathbf{x},\mathbf{y},\omega)\nabla p_{\mathrm{I}}(y_1,0,y_3,\omega)\cdot\mathbf{n}d\mathrm{S}(\mathbf{y}). \\ &= -\int_{-\infty}^{\infty} dy_3 \int_{-\ell}^{0} \frac{\partial p_{\mathrm{I}}}{\partial y_2}(y_1,0,y_3,\omega)\Big[G(\mathbf{x},\mathbf{y},\omega)\Big]\, dy_1 \end{aligned} \tag{3}$$

where

$$\Big[G(\mathbf{x},\mathbf{y},\omega)\Big] = G(\mathbf{x},y_1,+0,y_3,\omega) - G(\mathbf{x},y_1,-0,y_3,\omega) \tag{4}$$

is the jump in the value of G across the airfoil. The pressure p_{I} is equal to that which would be produced by the turbulence if the airfoil were imagined to be temporarily removed; it can be expressed in terms of the boundary layer 'blocked surface pressure', and equation (3) represents the edge noise in terms of the *scattering* of this pressure by the edge.

1.3. GREEN'S FUNCTION

1.3.1 Zeroth order approximations

At low Mach numbers the trailing edge interaction noise tends to be dominated by contributions to the integrals in (1) from the immediate neighborhood of the edge region. The wavelength of the sound $\sim \delta/M$, where δ is a length that characterizes the eddy size near the edge, and may in practice be of the order of the boundary layer thickness or the thickness h of the airfoil. In either case the acoustic wavelength greatly exceeds h when $M \ll 1$, which implies that the turbulence responsible for the edge noise is always very much closer than an acoustic wavelength from the edge. Then the nondimensional source distance $\kappa_o\sqrt{y_1^2+y_2^2} \sim \sqrt{y_1^2+y_2^2}/\text{acoustic wavelength} \ll 1$. When the observation point $\mathbf{x}$ is in the acoustic far field and $\mathbf{y}$ is within the source region, Green's function can then be expanded in terms of this small parameter:

$$G(\mathbf{x},\mathbf{y},\omega) = G_0(\mathbf{x},\mathbf{y},\omega) + G_1(\mathbf{x},\mathbf{y},\omega) + \ldots. \tag{5}$$

In the particular case of an airfoil whose chord ℓ is *acoustically compact* ($\kappa_o\ell \ll 1$) we find for $\kappa_o\sqrt{y_1^2+y_2^2} \ll 1$ [14]

$$G_0(\mathbf{x},\mathbf{y},\omega) = \frac{-e^{i\kappa_o|\mathbf{x}-y_3\mathbf{i}_3|}}{4\pi|\mathbf{x}-y_3\mathbf{i}_3|}, \quad G_1(\mathbf{x},\mathbf{y},\omega) = \frac{i\kappa_o \sin\psi \sin\theta \sqrt{\ell}\varphi^*(\mathbf{y})e^{i\kappa_o|\mathbf{x}-y_3\mathbf{i}_3|}}{4\pi|\mathbf{x}-y_3\mathbf{i}_3|}, \tag{6}$$

$$|\mathbf{x} - y_3\mathbf{i}_3| \to \infty,$$

where $\mathbf{i}_3$ is a unit vector parallel to the airfoil span (in the positive x_3-direction). If $r = \sqrt{x_1^2+x_2^2}$ denotes the observer distance from the edge of the airfoil (the x_3-axis), then (r,θ) are the polar coordinates of the observer position relative to a plane $x_3 =$ constant, i.e. $(x_1,x_2) = r(\cos\theta,\sin\theta)$; $\psi = \sin^{-1}(r/|\mathbf{x}|)$ is the angle between the observer direction $\mathbf{x}$ and the edge (see Figure 1b). The function $\varphi^*(\mathbf{y}) \equiv \varphi^*(y_1,y_2)$ of the source position $\mathbf{y}$ is a solution of Laplace's equation that may be interpreted physically as the velocity potential of ideal, incompressible flow around the edge (in the anticlockwise direction), and therefore depends on the geometrical shape of the edge. At source distances $\sqrt{y_1^2+y_2^2}$ from the edge that are large compared to the airfoil thickness h but small compared to the chord ℓ, $\varphi^*(\mathbf{y})$ must tend to the following expression for the potential of flow around a rigid *half-plane*:

$$\varphi^*(\mathbf{y}) \to \sqrt{r'}\sin(\theta'/2), \quad h \ll r' \ll \ell, \quad \text{where } (y_1,y_2) = r'(\cos\theta',\sin\theta'). \tag{7}$$

In the opposite extreme in which $\kappa_o \ell \to \infty$, when the airfoil chord is semi-infinite, the zeroth order component $G_0(\mathbf{x}, \mathbf{y}, \omega)$ in the expansion (5) is identical with that in (6) for the compact airfoil, but [14, 15]

$$G_1(\mathbf{x}, \mathbf{y}, \omega) = \frac{-\sqrt{\kappa_o} \sin^{\frac{1}{2}} \psi \sin\left(\frac{\theta}{2}\right) \varphi^*(\mathbf{y}) e^{i\kappa_o |\mathbf{x} - y_3 \mathbf{i}_3|}}{\pi \sqrt{2\pi i} |\mathbf{x} - y_3 \mathbf{i}_3|}, \quad \kappa_o \ell \to \infty, \quad \kappa_o \sqrt{y_1^2 + y_2^2} \ll 1. \tag{8}$$

In both limits G_0 represents the sound produced by a point source at $\mathbf{y}$ when scattering by the airfoil is neglected. The component G_1 gives the first correction due to the presence of the edge in the nearfield of the source, and supplies the leading approximation to the edge noise when used in equations (1) or (3).

Without loss of generality it will be assumed in what follows that the turbulence edge sources are located in the neighborhood of the origin O. The notation may then be simplified at the outset by setting $y_3 = 0$ in the equations (6) and (8). It may also be noted that $\sin\psi \sin\theta \equiv \cos\Theta$ in (6), where Θ is the angle between the radiation direction $\mathbf{x}$ and the nominal airfoil normal (the positive x_2-axis). In the compact limit the term G_1 accordingly represents an acoustic dipole orientated in the direction of the mean lift, in accordance with Curle's [21] theory.

1.3.2 Single scattering approximation

To bridge the extensive frequency interval between the approximations (6) and (8) occupied by airfoils of large but finite chord ℓ we introduce the notation

$$G(\mathbf{x}, \mathbf{y}, \omega) = G_1(\mathbf{x}, \mathbf{y}, \omega) + G_{\mathrm{LE}}(\mathbf{x}, \mathbf{y}, \omega) + G_{\mathrm{TE}}(\mathbf{x}, \mathbf{y}, \omega). \tag{9}$$

Here and henceforth the zeroth order, monopole component G_0 is discarded, since it plays no role in the production of edge noise. The components G_{LE}, G_{TE} will respectively represent additional contributions to G that may be associated with scattering at the leading and trailing edges of the airfoil. These terms arise in the following way.

For an airfoil of large chord we take G_1 in equation (9) to be defined by equation (8) (with $y_3 = 0$) for an airfoil with semi-infinite chord. This represents an acoustic disturbance whose wavelength is much larger than the airfoil thickness ($\kappa_o h \ll 1$) propagating as a function of $\mathbf{x}$ in the presence of an airfoil of semi-infinite chord. It therefore produces scattered waves at the leading edge, which are in turn scattered at the trailing edge and subsequently rescattered at the leading edge, etc. The functions G_{LE} and G_{TE} are defined

to account for the aggregate contributions from the leading and trailing edges of all of these scattering events.

Because $\kappa_o h \ll 1$, multiple scattering at the edges can be calculated by replacing the airfoil by one of zero thickness. Furthermore, as implied in the previous paragraph, the scattering calculation for, say, the leading edge is performed by assuming the zero-thickness airfoil to extend infinitely far downstream from the edge (to be *semi-infinite*); the resulting scattered field is then corrected at the trailing edge by a similar calculation performed, again, for a semi-infinite airfoil. Repeated application of this procedure and summation over all scattered contributions from the leading and trailing edges will then yield $G_{\rm LE}$, $G_{\rm TE}$. The method is identical to that used by Schwarzschild [28] for the simpler, two-dimensional problem of the diffraction by a slit of a normally incident plane wave, and is also discussed by Landahl in connection with two-dimensional gust loading of an airfoil [29].

The calculation can be carried out in full in terms of an expansion parameter $\sim 1/\kappa_o \ell \sin\psi$, which is required to be sufficiently small. The resulting multiple scattering expansion turns out to be analytic in κ_o in the region $|\kappa_o|\ell \sin\psi > 0.125$ of the *upper* complex plane, which suggests that the initial high frequency approximation can be analytically continued to more modest frequencies. On this basis we shall postulate the existence of a smooth interpolation with the (*compact*) very low frequency approximation of equation (6). The details of the calculation are straightforward, and will be illustrated by consideration of the leading edge scattered field $G_{\rm LE}$.

The zeroth order approximation G_1 (equation (8) with $y_3 = 0$) is first expressed as the following Fourier integral on the upper and lower surfaces of the zero thickness airfoil in the vicinity of the leading edge at $x_1 = -\ell$:

$$G_1(\mathbf{x},\mathbf{y},\omega) \equiv \frac{-\sqrt{\kappa_o}\sin^{\frac{1}{2}}\psi \sin\left(\frac{\theta}{2}\right)\varphi^*(\mathbf{y})e^{i\kappa_o|\mathbf{x}|}}{\pi\sqrt{2\pi i}|\mathbf{x}|}$$

$$\approx \frac{-\mathrm{sgn}(x_2)\varphi^*(\mathbf{y})e^{\frac{i\pi}{4}}}{(2\pi)^2\sqrt{\pi}} \iint_{-\infty}^{\infty} \frac{e^{i(kx_1+k_3x_3)}}{\sqrt{\bar{\kappa}_o + k}} dk dk_3, \quad \bar{\kappa}_o = \sqrt{\kappa_o^2 - k_3^2}, \ \kappa_o\ell \gg 1, \quad (10)$$

where $\mathrm{sgn}(x_2) = \pm 1$ according as $x_2 = \pm 0$, and the radiation condition requires that the imaginary part of $\bar{\kappa}_o = \sqrt{\kappa_o^2 - k_3^2}$ should be positive.

The interaction of G_1 with the leading edge of the airfoil may now be cast in terms of a diffraction problem for each Fourier component proportional to $\mathrm{sgn}(x_2)e^{i(kx_1+k_3x_3)}$. The

diffracted field can be determined exactly when the airfoil is regarded as semi-infinite (when the trailing edge is moved to $x_1 = +\infty$). The routine details of the calculation are discussed at great length by Noble [30], and it is sufficient here to quote the final form of the scattered field. Denoting this *first scattered* contribution from the leading edge by $G^1_{\rm LE}$, we find

$$G^1_{\rm LE}(\mathbf{x},\mathbf{y},\omega) = \frac{-{\rm sgn}(x_2)\varphi^*(\mathbf{y}){\rm e}^{-\frac{i\pi}{4}}}{(2\pi)^2\sqrt{\pi}} \iiint_{-\infty}^{\infty} \frac{\sqrt{\bar\kappa_0 - k}\,{\rm e}^{i\{k_1x_1' + k_3x_3 + \gamma(k_1,k_3)|x_2| - k\ell\}}}{\sqrt{\bar\kappa_0 + k}\sqrt{\bar\kappa_0 - k_1}(k_1 - k + i0)} dk_1 dk_3 dk, \tag{11}$$

where $x_1' = x_1 + \ell$, and the branch of $\gamma(k_1,k_3) = \sqrt{\kappa_0^2 - k_1^2 - k_3^2}$ with positive imaginary part is taken to satisfy the radiation condition.

The next step is to consider the interaction of this wave with the trailing edge. If, however, all such higher order interactions are neglected we shall obtain a *single scattering* approximation to $G(\mathbf{x},\mathbf{y},\omega)$. This corresponds to the approximation used by Amiet [1, 18, 19], and we shall pause to obtain its explicit representation when the observer position $\mathbf{x}$ moves to the acoustic far field of the airfoil. This is done by first evaluating the integrations with respect to k_1 and k_3 in (11) by the method of stationary phase [14], which supplies

$$G^1_{\rm LE}(\mathbf{x},\mathbf{y},\omega) \approx \frac{\sqrt{2\kappa_0}\varphi^*(\mathbf{y})\sin^{\frac{1}{2}}\psi' \cos\left(\frac{\theta'}{2}\right){\rm e}^{i(\kappa_0|\mathbf{x}'| + \frac{i\pi}{4})}}{(2\pi)^2\sqrt{\pi}|\mathbf{x}'|}$$
$$\times \int_{-\infty}^{\infty} \frac{\sqrt{\kappa_0\sin\psi' - k}\,{\rm e}^{-ik\ell}dk}{\sqrt{\kappa_0\sin\psi' + k}(\kappa_0\sin\psi'\cos\theta' - k + i0)}, \qquad \kappa_0|\mathbf{x}'| \to \infty, \tag{12}$$

where $\mathbf{x}' = (x_1 + \ell, x_2, x_3)$ and the corresponding angles ψ', θ' are defined by analogy with the angles ψ, θ of Figure 1b, but with the origin at the leading edge.

This formula is simplified further by noting that, when $|\mathbf{x}| \gg \ell$ we can replace $\mathbf{x}'$ by $\mathbf{x}$ in the denominator, and the angles $\psi' \to \psi$, $\theta' \to \theta$. When $\kappa_0\ell$ is large the principal contribution to the remaining integral is from the neighborhood of the branch point of the integrand at $k = -\kappa_0\sin\psi' \to -\kappa_0\sin\psi$. We can therefore set $\sqrt{\kappa_0\sin\psi' - k} = \sqrt{2\kappa_0\sin\psi}$ in the numerator, but, apart from replacing ψ', θ' by ψ, θ, the denominator must be left intact, because both terms can be arbitrarily small near the branch cut when $\theta \to \pi$. In this limit the pole of the integrand produces the forward scattered wave needed to cancel the incident wave (10) on the upstream extension of the airfoil. However, it is not necessary to make any further approximations, because when $\sqrt{\kappa_0\sin\psi' - k}$ is replaced by $\sqrt{2\kappa_0\sin\psi}$ the integral can be evaluated in closed form in terms of the error function ${\rm erf}(z) = \frac{2}{\sqrt{\pi}}\int_0^z {\rm e}^{-\xi^2}d\xi$. When the result is combined with the zeroth order term (10) we obtain the following *single scattering* approximation to the Green's function

$$G(\mathbf{x},\mathbf{y},\omega) \approx G_1(\mathbf{x},\mathbf{y},\omega) + G^1_{\rm LE}(\mathbf{x},\mathbf{y},\omega)$$

$$\approx \frac{-\sqrt{\kappa_0}\varphi^*(\mathbf{y})\sin^{\frac{1}{2}}\psi}{\pi\sqrt{2\pi i}|\mathbf{x}|}\left(\sin\frac{\theta}{2}e^{i\kappa_0|\mathbf{x}|}\right.$$
$$\left. - e^{i\kappa_0(|\mathbf{x}'|-\ell\sin\psi\cos\theta)}\left[1-\mathrm{erf}\left(e^{-\frac{i\pi}{4}}\sqrt{2\kappa_0\ell\sin\psi\cos^2\frac{\theta}{2}}\right)\right]\right), \quad \kappa_0|\mathbf{x}|\to\infty. \tag{13}$$

For purposes of computation the error function of complex argument may be expressed in terms of the real-valued *Fresnel integral auxiliary functions* $f(x)$, $g(x)$ defined in §7.3 of [31], in which case the single scattering approximation becomes

$$G(\mathbf{x},\mathbf{y},\omega) \approx \frac{-\sqrt{\kappa_0}\varphi^*(\mathbf{y})\sin^{\frac{1}{2}}\psi}{\pi\sqrt{2\pi i}|\mathbf{x}|}\left[\sin\frac{\theta}{2}e^{i\kappa_0|\mathbf{x}|}\right.$$
$$\left. - \sqrt{2}e^{i\{\kappa_0(|\mathbf{x}'|+\ell\sin\psi)-\frac{\pi}{4}\}}\mathcal{F}\left(2\sqrt{\frac{\kappa_0\ell\sin\psi\cos^2\frac{\theta}{2}}{\pi}}\right)\right], \quad \kappa_0|\mathbf{x}|\to\infty. \tag{14}$$

where $\mathcal{F}(x) = g(x) + if(x)$.

1.3.3 Multiple scattering

Return now to the multiple scattering calculation of $G_{\rm LE}$. First order scattering at the leading edge produces the acoustic field $G^1_{\rm LE}$ given by (11). A diffraction calculation must be performed to determine the field produced when this wave is scattered back to the leading edge from the trailing edge. To do this the representation (11) is first used to simplify the expression for the first order wave incident on the trailing edge by replacing the integrations with respect to k and k_1 by the corresponding leading order term in the asymptotic expansion for $\kappa_0\ell \gg 1$, which is readily found in the form

$$G^1_{\rm LE}(\mathbf{x},\mathbf{y},\omega) \approx \frac{-\mathrm{sgn}(x_2)\varphi^*(\mathbf{y})e^{-\frac{i\pi}{4}}}{\pi\sqrt{2\pi}}\int_{-\infty}^{\infty}\sqrt{\bar\kappa_0}\,\epsilon\,e^{i(\bar\kappa_0 x_1+k_3x_3)}dk_3, \quad x_2=\pm 0, \tag{15}$$

where

$$\epsilon = \frac{e^{2i\bar\kappa_0\ell}}{2\pi i\bar\kappa_0\ell}. \tag{16}$$

A diffraction calculation is then performed for each Fourier component proportional to $e^{i(\bar\kappa_0 x_1+k_3x_3)}$ incident on the trailing edge, as before. The net result of these calculations is

just the first term $G^1_{\rm TE}(\mathbf{x},\mathbf{y},\omega)$, say, in the sequence of waves scattered from the trailing edge. Just above and below the airfoil this wave is found to be given by

$$G^1_{\rm TE}(\mathbf{x},\mathbf{y},\omega) = \frac{-{\rm sgn}(x_2)\varphi^*(\mathbf{y}){\rm e}^{\frac{i\pi}{4}}}{(2\pi)^2\sqrt{\pi}} \iint_{-\infty}^{\infty} \frac{2\bar\kappa_{\rm o}\epsilon\, {\rm e}^{i(kx_1+k_3x_3)}}{\sqrt{\bar\kappa_{\rm o}+k}(k-\bar\kappa_{\rm o}-i0)} dkdk_3, \quad x_2 = \pm 0. \tag{17}$$

The integrand can be simplified by replacing $k-\bar\kappa_{\rm o}-i0$ by $-2\bar\kappa_{\rm o}$ when $x_1 \sim -\ell$, because when $\kappa_{\rm o}\ell$ is large the main contribution from the integration with respect to k is from the vicinity of the branch point at $k=-\bar\kappa_{\rm o}$. When the result is combined with (10) we then find, near the leading edge,

$$G_1(\mathbf{x},\mathbf{y},\omega) + G^1_{\rm TE}(\mathbf{x},\mathbf{y},\omega) \approx \frac{-{\rm sgn}(x_2)\varphi^*(\mathbf{y}){\rm e}^{\frac{i\pi}{4}}}{(2\pi)^2\sqrt{\pi}} \iint_{-\infty}^{\infty} \frac{{\rm e}^{i(kx_1+k_3x_3)}}{\sqrt{\bar\kappa_{\rm o}+k}}\,[1-\epsilon]\, dkdk_3. \tag{18}$$

It is now clear that repeated application of the calculations leading to this result will produce the following expansion for the whole of the field incident on the leading edge

$$\begin{aligned} & G_1(\mathbf{x},\mathbf{y},\omega) + G^1_{\rm TE}(\mathbf{x},\mathbf{y},\omega) + G^2_{\rm TE}(\mathbf{x},\mathbf{y},\omega) + \cdots \\ &= G_1(\mathbf{x},\mathbf{y},\omega) + G_{\rm TE}(\mathbf{x},\mathbf{y},\omega) \\ &\approx \frac{-{\rm sgn}(x_2)\varphi^*(\mathbf{y}){\rm e}^{\frac{i\pi}{4}}}{(2\pi)^2\sqrt{\pi}} \iint_{-\infty}^{\infty} \frac{{\rm e}^{i(kx_1+k_3x_3)}}{\sqrt{\bar\kappa_{\rm o}+k}} \sum_{n=0}^{\infty} (-\epsilon)^n\, dkdk_3, \\ & \qquad\qquad x_1 \sim -\ell,\ x_2 = \pm 0. \end{aligned} \tag{19}$$

Now $\epsilon = {\rm e}^{2i\bar\kappa_{\rm o}\ell}/2\pi i\bar\kappa_{\rm o}\ell$, so that the series converges absolutely for $|\bar\kappa_{\rm o}|\ell > 1/2\pi$ for real values of $\bar\kappa_{\rm o}$, and everywhere in ${\rm Im}\,\bar\kappa_{\rm o} > 0$ outside a region enclosing the origin bounded by the curve $2\pi|\bar\kappa_{\rm o}|\ell = \exp(-2{\rm Im}\,\bar\kappa_{\rm o}\ell)$. In the region of convergence

$$\sum_{n=0}^{\infty}(-\epsilon)^n \equiv \sum_{n=0}^{\infty}\left(\frac{-{\rm e}^{2i\bar\kappa_{\rm o}\ell}}{2\pi i\bar\kappa_{\rm o}\ell}\right)^n = \left(1+\frac{{\rm e}^{2i\bar\kappa_{\rm o}\ell}}{2\pi i\bar\kappa_{\rm o}\ell}\right)^{-1}, \tag{20}$$

so that equation (19) becomes

$$G_1(\mathbf{x},\mathbf{y},\omega) + G_{\rm TE}(\mathbf{x},\mathbf{y},\omega) \approx \frac{-{\rm sgn}(x_2)\varphi^*(\mathbf{y}){\rm e}^{\frac{i\pi}{4}}}{(2\pi)^2\sqrt{\pi}} \iint_{-\infty}^{\infty} \frac{{\rm e}^{i(kx_1+k_3x_3)}}{\sqrt{\bar\kappa_{\rm o}+k}(1+{\rm e}^{2i\bar\kappa_{\rm o}\ell}/2\pi i\bar\kappa_{\rm o}\ell)} dkdk_3. \tag{21}$$

The component $G_{\rm LE}$ of Green's function is produced by diffraction of this field at the leading edge. Performing the diffraction calculation in the manner already discussed, and considering the limiting form in the acoustic far field, where $\kappa_{\rm o}|\mathbf{x}| \gg 1$, we accordingly find

$$G_{\rm LE}(\mathbf{x},\mathbf{y},\omega) \approx \frac{\sqrt{\kappa_o}\sin^{\frac{1}{2}}\psi\varphi^*(\mathbf{y})e^{i\kappa_o(|\mathbf{x}'|-\ell\sin\psi\cos\theta)}}{\pi\sqrt{2\pi i}|\mathbf{x}|(1+e^{2i\kappa_o\ell\sin\psi}/2\pi i\kappa_o\ell\sin\psi)}\left[1-\mathrm{erf}\left(e^{-\frac{i\pi}{4}}\sqrt{2\kappa_o\ell\sin\psi\cos^2\frac{\theta}{2}}\right)\right]$$

$$= \frac{\sqrt{\kappa_o}\sin^{\frac{1}{2}}\psi\varphi^*(\mathbf{y})e^{i\kappa_o(|\mathbf{x}'|+\ell\sin\psi)}}{i\pi^{\frac{3}{2}}|\mathbf{x}|(1+e^{2i\kappa_o\ell\sin\psi}/2\pi i\kappa_o\ell\sin\psi)}\mathcal{F}\left(2\sqrt{\frac{\kappa_o\ell\sin\psi\cos^2\frac{\theta}{2}}{\pi}}\right), \quad \kappa_o|\mathbf{x}|\to\infty. \tag{22}$$

Similarly, the trailing edge component $G_{\rm TE}(\mathbf{x},\mathbf{y},\omega)$ is produced by the diffraction of $G_{\rm LE}(\mathbf{x},\mathbf{y},\omega)$ at the trailing edge, and is found by the same procedure to be given in the acoustic far field by

$$G_{\rm TE}(\mathbf{x},\mathbf{y},\omega) \approx \frac{-\varphi^*(\mathbf{y})e^{i\kappa_o\{|\mathbf{x}|+\ell\sin\psi(1+\cos\theta)\}}}{2\pi^2\sqrt{\ell}|\mathbf{x}|(1+e^{2i\kappa_o\ell\sin\psi}/2\pi i\kappa_o\ell\sin\psi)}\left[1-\mathrm{erf}\left(e^{-\frac{i\pi}{4}}\sqrt{2\kappa_o\ell\sin\psi\sin^2\frac{\theta}{2}}\right)\right]$$

$$= \frac{-\varphi^*(\mathbf{y})e^{i\kappa_o(|\mathbf{x}|+2\ell\sin\psi)}}{\pi^2\sqrt{2i\ell}|\mathbf{x}|(1+e^{2i\kappa_o\ell\sin\psi}/2\pi i\kappa_o\ell\sin\psi)}\mathcal{F}\left(2\sqrt{\frac{\kappa_o\ell\sin\psi\sin^2\frac{\theta}{2}}{\pi}}\right), \quad \kappa_o|\mathbf{x}|\to\infty. \tag{23}$$

In these asymptotic expressions the principal contribution of the dimensionless quantity $\bar{\kappa}_o\ell$ in, say, the denominator of the integrand of (21), has the value $\kappa_o\ell\sin\psi$. This implies that, for the acoustic far field, the expansion (20) is formally convergent in the upper $\kappa_o\ell\sin\psi$-plane in the region indicated in Figure 2, outside the curve $2\pi|\kappa_o|\ell\sin\psi = \exp(-2\mathrm{Im}\,\kappa_o\ell\sin\psi)$. In particular, the expansion ceases to be valid in radiation directions $\psi\sim 0,\ \pi$ parallel to the airfoil span.

1.4. TRAILING EDGE NOISE

1.4.1 Frequency dependence of Green's function

At each step in the above sequence of diffraction problems the incident wave has effectively been approximated by the first term in its asymptotic expansion in powers of $1/\sqrt{\kappa_0 \ell \sin\psi}$. Because of this, as soon as the approximation goes beyond $G \approx G_1 + G^1_{\rm LE} + G^1_{\rm TE}$ the neglected terms are formally of the same order as terms retained in $G^n_{\rm LE}$, $G^n_{\rm TE}$, $n \geq 2$. The procedure we have used corresponds to the retention of a certain 'principal subseries' of terms from a complete expansion of $G_{\rm LE}$ and $G_{\rm TE}$ in powers of $1/\sqrt{\kappa_0 \ell \sin\psi}$; each member of the subseries describes the leading order effect of edge diffraction at each stage. The procedure is familiar in quantum mechanical calculations of multiple scattering [32 - 34], where 'Feynman diagrams' are used to extract convergent subseries of this kind.

To assess the accuracy of the various approximations the ratio $|G(\mathbf{x},\mathbf{y},\omega)/G_1(\mathbf{x},\mathbf{y},\omega)|$ is plotted against $\kappa_0 \ell \sin\psi$ in Figure 3 for typical cases $\theta = 90°,\ 135°$ for the three approximations:

$$G(\mathbf{x},\mathbf{y},\omega) = \begin{cases} G_1(\mathbf{x},\mathbf{y},\omega) + G^1_{\rm LE}(\mathbf{x},\mathbf{y},\omega) \\ G_1(\mathbf{x},\mathbf{y},\omega) + G^1_{\rm LE}(\mathbf{x},\mathbf{y},\omega) + G^1_{\rm TE}(\mathbf{x},\mathbf{y},\omega) \\ G_1(\mathbf{x},\mathbf{y},\omega) + G_{\rm LE}(\mathbf{x},\mathbf{y},\omega) + G_{\rm TE}(\mathbf{x},\mathbf{y},\omega), \end{cases}$$

where G_1 is the half-plane Green's function in the first line of equation (10). The first is the single scattering approximation (14), the second includes in addition one scattering term from the trailing edge (obtained by replacing the factor $(1+\mathrm{e}^{2i\kappa_0 \ell \sin\psi}/2\pi i \kappa_0 \ell \sin\psi)$ by unity in the denominators of (22) and (23)), the third is the multiple scattering approximation given by (22) and (23). The comparison is made in the acoustic far field where

$$|\mathbf{x}'| \approx |\mathbf{x}| + \ell \sin\psi \cos\theta.$$

The function $\mathcal{F}(x) = g(x) + if(x)$ is conveniently computed using the rational approximations given in §7.3 of [31], which are quoted here for ease of reference:

$$f(x) = \frac{1 + 0.926x}{2 + 1.792x + 3.104x^2}, \quad g(x) = \frac{1}{2 + 4.142x + 3.492x^2 + 6.670x^3},$$

where the absolute errors for $0 \leq x \leq \infty$ are no larger than 0.002.

All three approximations agree at high frequencies ($\kappa_0 \ell \sin\psi > 7$). The effective agreement between the double and multiple scattering approximations when $\kappa_0 \ell \sin\psi$

exceeds about 0.7 suggests that the multiple scattering, 'principal subseries' approximation is likely to provide an excellent overall approximation at these frequencies.

At very low frequencies the airfoil chord becomes acoustically compact, and trailing edge noise will be governed by the approximation (6) for $G_1(\mathbf{x}, \mathbf{y}, \omega)$. The broken curve in Figure 4 is a plot of the ratio

$$\left| \frac{(G_1(\mathbf{x}, \mathbf{y}, \omega))_{\text{compact}}}{(G_1(\mathbf{x}, \mathbf{y}, \omega))_{\text{half-plane}}} \right|$$

for $\theta = 90°$ in the acoustic far field. The solid curve is a possible smooth interpolation over all frequencies which agrees with the high frequency multiple scattering solution (dotted) for $\kappa_0 \ell \sin\psi > 0.6$. Similar interpolations valid over $0 < \kappa_0 \ell < \infty$ are readily constructed for other radiation directions.

The finite chord of the airfoil can modify significantly the *directivity* of the edge noise relative to the familiar *cardioid* pattern associated with a semi-infinite airfoil. This is illustrated in Figure 5 for $\psi = 90°$ for $\kappa_0 \ell = 1,\ 5,\ 10$ and 50. The heavy curves are polar plots of the *linear* field strength (normalized to the same maximum value); in each case the light curve corresponds to the $\sin\left(\frac{\theta}{2}\right)$ directionality for the half-plane ($\kappa_0 \ell = \infty$). At the lowest frequency shown in Figure 5 ($\kappa_0 \ell = 1$) the radiation peaks in directions normal to the airfoil, and the directivity coincides with that for a *dipole* source orientated in the x_2-direction. Multiple lobes develop as the frequency increases, and the directivity tends in an oscillatory manner towards that for the half-plane. In all cases there are radiation nulls in the directions $\theta = 0°$ and $180°$, respectively downstream and upstream of the airfoil.

1.4.2 Frequency spectrum of trailing edge noise

The influence of multiple scattering on the trailing edge noise frequency spectrum is evidently independent of the trailing edge geometry. The prediction of the edge noise spectrum for a finite chord airfoil is obtained from that predicted for an airfoil of semi-infinite chord merely by multiplication by the ratio

$$\left| \frac{G(\mathbf{x}, \mathbf{y}, \omega)}{(G_1(\mathbf{x}, \mathbf{y}, \omega))_{\text{half-plane}}} \right|^2$$

where $G(\mathbf{x}, \mathbf{y}, \omega)$ is an appropriate interpolation between the low and high frequency representations, such as that depicted in Figure 4.

To illustrate the situation at very low Mach numbers, let $\Phi_\infty(\mathbf{x}, \omega)$ denote the frequency pressure spectrum of the sound at the far field point $\mathbf{x}$ predicted for turbulent flow from

the edge of a rigid half-plane. This particular case has been treated by many authors [3 - 5, 7 - 11] by means of the representation in terms of the boundary layer wall pressure given by equations (3) and (4) of §2. It will therefore be sufficient to present the following result from reference [14] for the spectrum of the far field sound ($|\mathbf{x}| \to \infty$) produced by turbulent flow over *one side* of the airfoil

$$\Phi_\infty(\mathbf{x},\omega) \approx a_0 M \left(\frac{\delta_* L}{|\mathbf{x}|^2}\right) \sin^2(\theta/2) \sin\psi \frac{\Phi_{pp}(\omega)}{\omega\delta_*/U}, \quad M = U/c_0 \ll 1, \quad a_0 = 0.035. \tag{24}$$

In this formula δ_* and $\Phi_{pp}(\omega)$ are respectively the boundary layer displacement thickness and the frequency spectrum of the wall pressure fluctuations just upstream of the edge, and L is the span of the airfoil wetted by the turbulence. We shall use the interpolation formula [14] (based on data collated by Chase [35])

$$\frac{(U/\delta_*)\Phi_{pp}(\omega)}{(\rho_o v_*^2)^2} = \frac{(\omega\delta_*/U)^2}{[(\omega\delta_*/U)^2 + \alpha_p^2]^{\frac{3}{2}}}, \quad \alpha_p = 0.12, \tag{25}$$

where v_* is the boundary layer friction velocity at the edge. The broken-line curve in Figure 6 is the corresponding prediction of the edge noise acoustic pressure spectrum $(U/\delta_*)\Phi_\infty(\mathbf{x},\omega)/[a_o(\rho_o v_*^2)^2 M(\delta_* L/|\mathbf{x}|^2)\sin^2(\theta/2)\sin\psi]$ for $\theta = \psi = 90°$.

The following parameter values are typical of model scale tests conducted in air and in associated numerical simulations [8 - 11, 24 - 26]

$$\frac{\ell}{\delta_*} \approx 78, \quad M = 0.09, \quad \text{so that} \quad \kappa_0\ell \equiv \frac{\omega\ell}{c_0} = M\frac{\ell}{\delta_*}\frac{\omega\delta_*}{U} \approx 7\frac{\omega\delta_*}{U}. \tag{26}$$

Using this to calculate $\kappa_0\ell$ in terms of $\omega\delta^*/U$, the acoustic pressure frequency spectrum for an airfoil of chord ℓ is given by

$$\Phi(\mathbf{x},\omega) = \Phi_\infty(\mathbf{x},\omega)\left|\frac{G(\mathbf{x},\mathbf{y},\omega)}{(G_1(\mathbf{x},\mathbf{y},\omega))_{\text{half-plane}}}\right|^2. \tag{27}$$

The normalized version of this spectrum is plotted as the solid curves in Figure 6 for the two radiation directions $\psi = 90°$ and $\theta = 90°$, 135°. Significant departures from the half-plane prediction $\Phi_\infty(\mathbf{x},\omega)$ occur for $\omega\delta_*/U < 0.4$; in particular spectral levels are reduced at frequencies below that of the spectral peak, which is shifter to higher frequencies.

1.5. CONCLUSION

Numerical simulations and model scale experimental studies of trailing edge noise at low Mach numbers frequently involve acoustic frequencies that are sufficiently small that the usual assumption that the airfoil chord may be regarded as semi-infinite becomes invalid. The results presented in this chapter indicate that errors in predictions of the edge noise acoustic pressure spectrum based on this model are possible at lower and intermediate frequencies, and in particular in the neighborhood of the spectral peak, which tends to be shifted to higher frequencies because of the reduced efficiency of edge noise production as the airfoil chord decreases relative to the acoustic wavelength. For the model scale tests reported in [8, 9, 11] and the numerical simulations in [24 - 26], the errors are likely to be significant when $\omega\delta_*/U$ is smaller than about 0.4. Considerable departures from the half-plane radiation directivity occur at all frequencies, but especially at reduced frequencies $\kappa_0\ell < 10$.

The approximation given in this chapter for the edge-source Green's function may be used to solve a variety of low Mach number aeroacoustic problems using the general solution given by equation (1). Of particular interest are those involving the interaction of discrete vortex structures with the leading or trailing edge. In general a preliminary calculation of the *incompressible* flow in the immediate vicinity of the airfoil must be performed to determine the time dependent distribution of the vorticity. For an impinging gust, for example, it would be necessary to take proper account of additional vorticity generated at the surface of the airfoil (e.g., at the trailing edge), and also of the evolution of the gust vorticity as it convects past the airfoil, especially in the non-uniform regions of the mean flow near the leading and trailing edges.

REFERENCES

1. R. K. Amiet 1974 *American Institute of Aeronautics and Astronautics Journal* **12**, 252 - 255. Compressibility effects in unsteady thin-airfoil theory.
2. J. E. Ffowcs Williams and L. H. Hall 1970 *Journal of Fluid Mechanics* **40**, 657 - 670. Aerodynamic sound generation by turbulent flow in the vicinity of a scattering half-plane.
3. D. M. Chase 1972 *Journal of the Acoustical Society of America* **52**, 1011 - 1023. Sound radiated by turbulent flow off a rigid hal-plane as obtained from a wavevector spectrum of hydrodynamic pressure.
4. K. L. Chandiramani 1974 *Journal of the Acoustical Society of America* **55**, 19 - 29. Diffraction of evanescent waves, with applications to aerodynamically scattered sound and radiation from unbaffled plates.
5. D. M. Chase 1975 *American Institute of Aeronautics and Astronautics Journal* **13**, 1041 - 1047. Noise radiated from an edge in turbulent flow.
6. R. K. Amiet 1976 *Journal of Sound and Vibration* **47**, 387 - 393. Noise due to turbulent flow past a trailing edge.
7. M. S. Howe 1978 *Journal of Sound and Vibration* **61**, 437 - 466. A review of the theory of trailing edge noise.
8. W. K. Blake 1983 in *Proceedings of the International Symposium on Turbulence Induced Vibrations and Noise of Structures*, (M. M. Sevik, editor). American Society of Mechanical Engineers, New York, pp 45 - 65. Excitation of plates and hydrofoils by trailing edge flows.
9. W. K. Blake 1986 *Mechanics of flow-induced sound and vibration*, Vol. 2: *Complex flow-structure interactions.* New York: Academic Press.
10. J. Gershfeld, W. K. Blake and C. W. Knisely 1988 *American Institute of Aeronautics and Astronautics Paper* 88-3826-CP Trailing edge flow and aerodynamic sound.
11. W. K. Blake and J. L. Gershfeld 1989 in *Lecture Notes in Engineering* 46 (Ed. M. Gad-el-Hak). Frontiers in Experimental Fluid Mechanics: The aeroacoustics of trailing edges.

12. T. F. Brooks, D. S. Pope and M. A. Marcolini 1989 *National Aeronautics and Space Administration Reference Publication No. 1218.* Airfoil self-noise and prediction.

13. D. G. Crighton 1991 Chapter 7 of *Aeroacoustics of Flight Vehicles: Theory and Practice* (Vol. 1). *National Aeronautics and Space Administration Reference Publication No. 1258.* Airframe noise.

14. M. S. Howe 1998 *Acoustics of Fluid-Structure Interactions*, Cambridge University Press.

15. M. S. Howe 1999 *Journal of Sound and Vibration* (in press). Trailing edge noise at low Mach numbers.

16. M. S. Howe 1998 Submitted to *Journal of Sound and Vibration.* Trailing edge noise at low Mach numbers. Part 2: Attached and separated edge flows.

17. J. J. Adamczyk 1974 *NASA Contractor Report No. 2395.* The passage of an infinite swept airfoil through an oblique gust.

18. R. K. Amiet 1975 *J. Sound Vib.* **41**, 407 - 420. Acoustic radiation from an airfoil in a turbulent stream.

19. R. K. Amiet 1986 *J. Sound Vib.* **107**, 487 - 506. Airfoil gust response and the sound produced by airfoil-vortex interaction.

20. R. Martinez and S. E. Widnall 1980 *AIAA J* **18**, 636 - 645. Unified aerodynamic-acoustic theory for a thin rectangular wing encountering a gust.

21. N. Curle 1955 *Proc. Roy. Soc. Lond.* **A231**, 505 - 514. The influence of solid boundaries upon aerodynamic sound.

22. R. K. Amiet 1975 *J. Sound Vib.* **47**, 387 - 393. Noise due to turbulent flow past a trailing edge.

23. R. K. Amiet 1975 *J. Sound Vib.* **57**, 305 - 306. Effect of the incidence surface pressure field on noise due to turbulent flow past a trailing edge.

24. M. Wang 1997 *Annual Research Briefs* 37 - 49, (Center for Turbulence Research, Stanford University). Progress in large-eddy simulation of trailing-edge turbulence and aeroacoustics.

25. M. Wang 1998 *Annual Research Briefs* 91 -106, (Center for Turbulence Research, Stanford University). Computation of trailing-edge noise at low mach number using LES and acoustic analogy.

26. M. Wang and P. Moin 1999 Submitted to *AIAA J.* Computation of trailing-edge noise using large-eddy simulation.

27. G. K. Batchelor 1967 *An introduction to fluid dynamics.* Cambridge University Press.

28. K. Schwarzschild 1901 *Math. Ann.* **55**, 177 - 247. Die Beugung und Polarisation des Lichts durch einen Spalt - I.

29. M. T. Landahl 1989 *Unsteady Transonic Flow.* Cambridge University Press (originally published by Pergamon Press, 1961).

30. B. Noble 1958 *Methods based on the Wiener-Hopf Technique.* London: Pergamon Press. (Reprinted 1988, Chelsea Publishing Company, New York.)

31. M. Abramowitz and I. A. Stegun (editors) 1970 *Handbook of Mathematical Functions* (ninth corrected printing), US Department of Commerce, National Bureau of Standards Applied Mathematics Series No.55.

32. U. Frisch 1966 *Ann. d'Astrophys.* **29**, 645 - 682. The propagation of sound in a random medium and stochastic equations. I. Part one.

33. U Frisch 1967 *Ann. d'Astrophys.*, **30**, 565 - 601. The propagation of sound in a random medium and stochastic equations. II. Applications.

34. Bharucha-Reid, A. T. 1968 (editor). *Probabilistic methods in Applied Mathematics*, Volume 1. New York: Academic Press.

35. D. M. Chase 1980 *J. Sound Vib.* **70**, 29 - 67. Modeling the wavevector-frequency spectrum of turbulent boundary layer wall pressure.

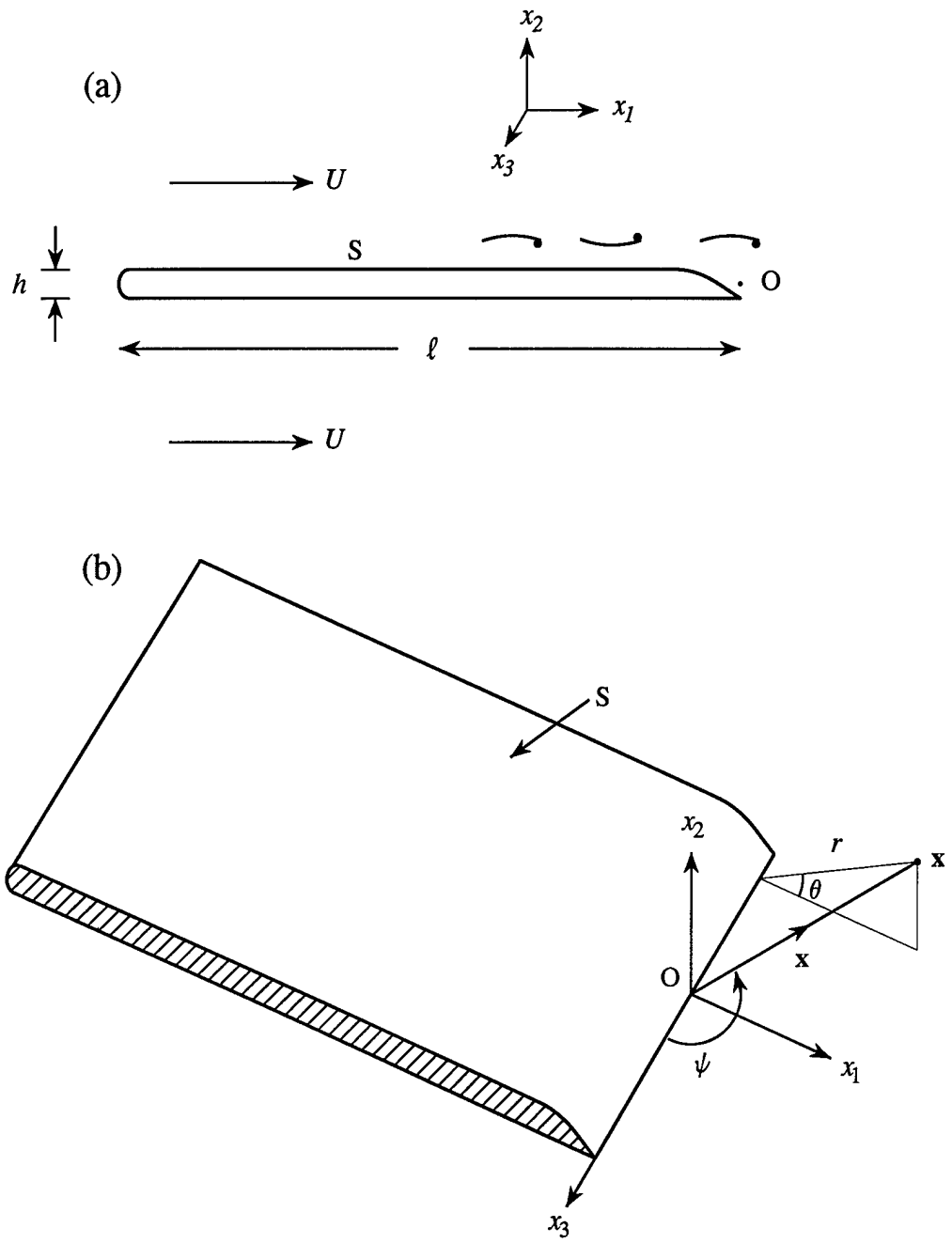

Figure 1. (a) Airfoil of thickness h and uniform chord ℓ with turbulent edge sources. (b) Coordinates defining the observer position in the acoustic far field.

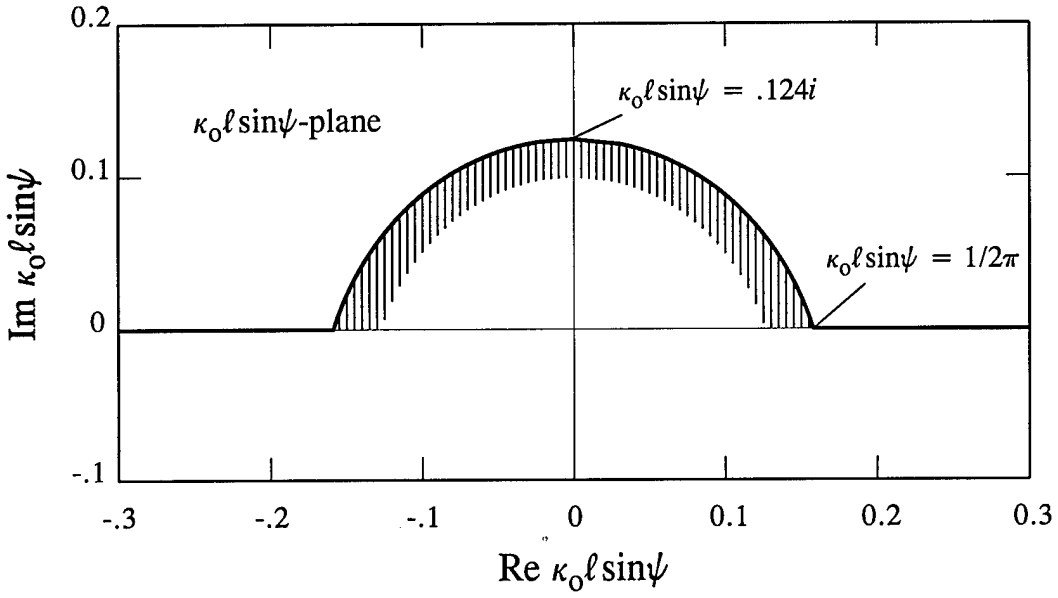

Figure 2. The series (20) converges in the upper complex $\kappa_o \ell \sin\psi$-plane outside the cross-hatched region.

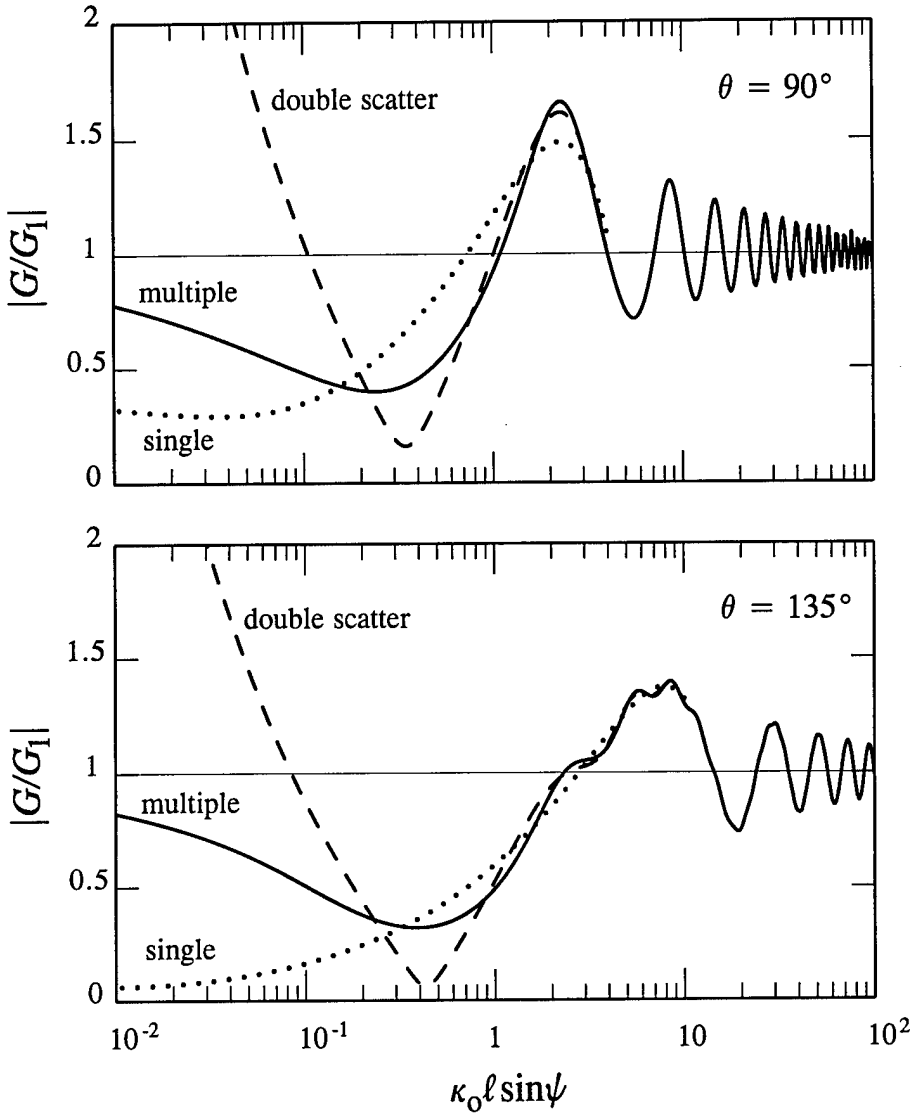

Figure 3. Comparison of single (• • •), double (– – –) and multiple (———) scattering approximations at $\theta = 90°,\ 135°$..

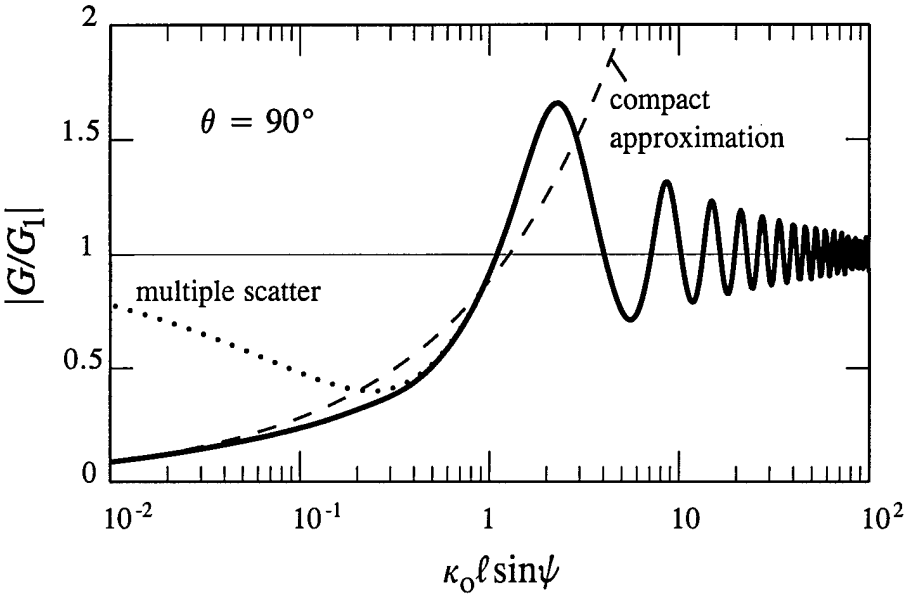

Figure 4. Interpolation (———) between the compact approximation (second of equation (6) with $y_3 = 0$) (– – –) and the high frequency multiple scattering approximation (9), (22), (23) (• • •).

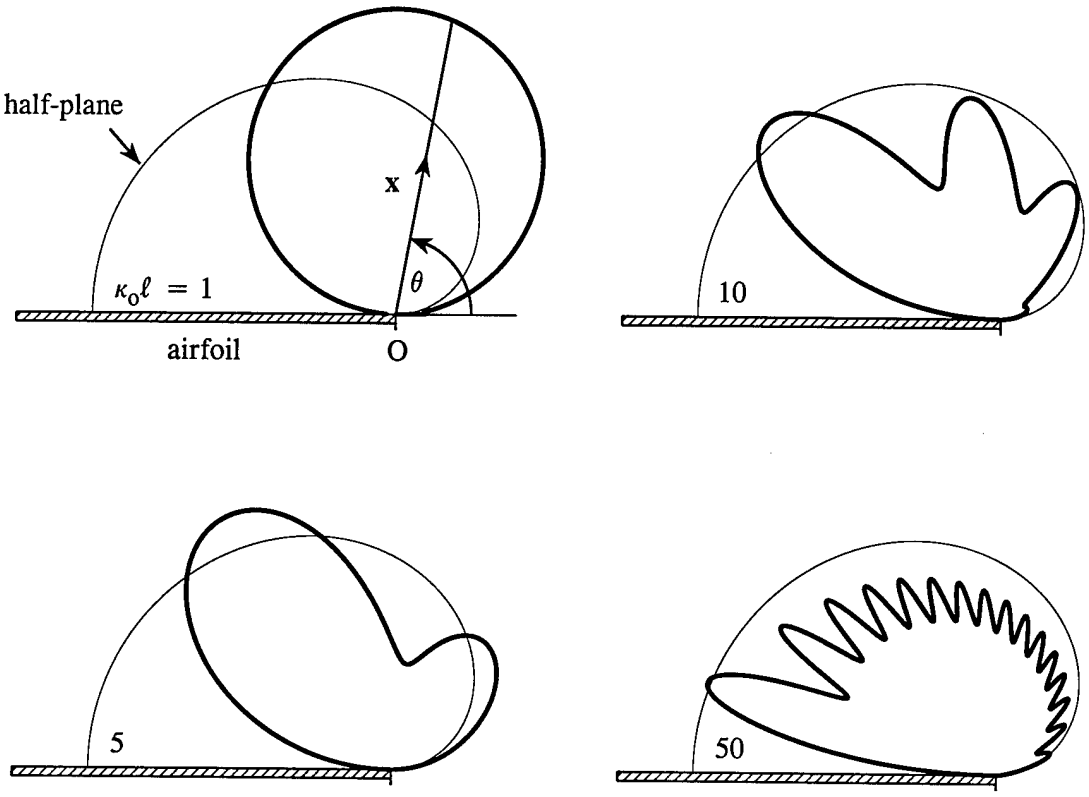

Figure 5. Linear directivity for $\psi = 90°$ compared with that for a half-plane.

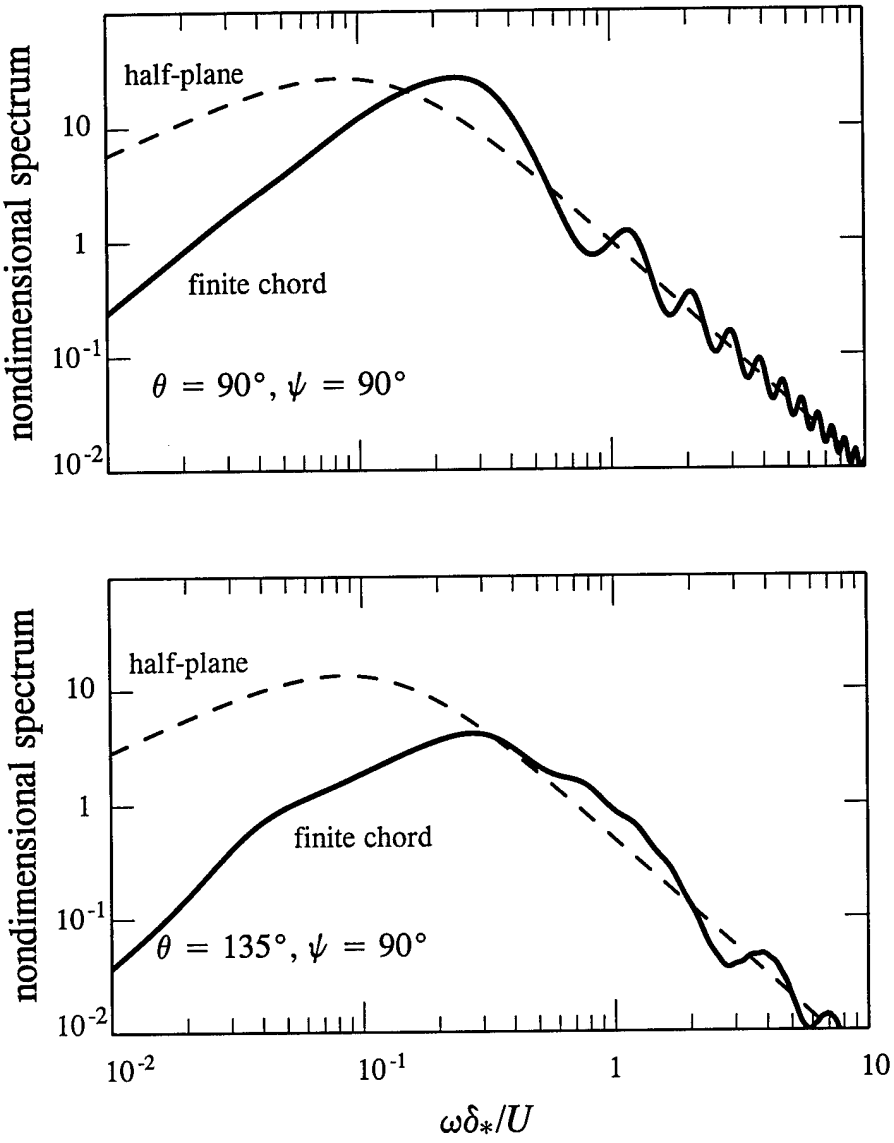

Figure 6. Comparison of the predicted edge noise spectrum (24) for the rigid half-plane $(U/\delta_*)\Phi_\infty(\mathbf{x},\omega)/[a_o(\rho_o v_*^2)^2 M(\delta_* L/|\mathbf{x}|^2)\sin^2(\theta/2)\sin\psi]$ with that for an airfoil of finite chord ℓ given by (27), when $\psi = 90°$ for $\theta = 90°$ and 135° and conditions (26).

CHAPTER 2

ON THE HYDROACOUSTICS OF A TRAILING EDGE WITH A DETACHED FLAP

SUMMARY

An analysis is made of the production of sound by low Mach number turbulent flow over the trailing edge of an airfoil with a single detached flap. An objective is to quantify the separate contributions to the production of sound by turbulence interacting with the trailing edge of the airfoil, the trailing edge of the flap, and with the leading edge of the flap. The side-edge noise of part-span flaps is not discussed.

An aeroacoustic Green's function is derived for an airfoil of large chord with a detached flap at relative angle of attack α ($\alpha^2 \ll 1$) when the chord of the flap is acoustically compact. Formulae are given for calculating the 'self-noise' produced at trailing edges by boundary layer instability; the efficiency of sound generation at the edge of the airfoil is shown to be typically at least 7dB larger than that produced at the trailing edge of the flap. The impingement noise generated by turbulence interacting with the flap leading edge is expressed in terms of an equivalent dipole source equal to the fluctuating flap-lift-force, acting at a distance ℓ_F to the rear of the main airfoil; ℓ_F is determined as a function of the flap dimensions, and does not normally exceed about twice the width h of the slot separating the airfoil and flap. The proximity of the dipole to the edge of the airfoil increases the efficiency of sound production by a factor proportional to $h/(\ell_F M)$ where $M \ll 1$ is the characteristic edge flow Mach number, and modifies the directivity of the sound. The Green's function can be used with data derived from direct numerical simulations of the unsteady hydrodynamic flow, and provides an effective means of calculating the radiation from a knowledge of the *incompressible* component of the flow in the edge region.

2.1. INTRODUCTION

The efficiency with which sound is generated by very low Mach number 'hydroacoustic' flows is so small that the unsteady motion in the source region is effectively indistinguishable from that of an incompressible fluid. Great caution must therefore be exercised in interpreting numerical predictions of the minute acoustic byproduct of the flow, and it is unwise to invest too much confidence in direct numerical simulations of sound production, which are often dominated by numerical rather than acoustic noise. It is particularly difficult, for example, to make reliable estimates of the sound produced by turbulence in the neighborhood of a solid surface whose radius of curvature is large relative to the acoustic wavelength. Both the amplitude and directionality of the sound are crucially dependent on the relative phasing of very small source components distributed over regions spanned by many acoustic wavelengths; such phase variations are largely indeterminate by conventional numerical procedures when the flow is effectively incompressible, and spurious noise predictions can result from the indiscriminate use of computed data in, say, Curle's [1] or Kirchhoff's [2] surface integral representation of the sound.

This chapter is concerned with the important special case of the generation of sound by low Mach number turbulent flow in the vicinity of the trailing edge of an airfoil whose chord is generally large relative to the acoustic wavelength. Numerical predictions in which Curle's equation [1] (or the Ffowcs Williams - Hawkings equation [3]) is used with airfoil surface data derived from an incompressible numerical simulation of the flow are known to be incorrect [4, 5]. Theoretical methods for studying this problem are usually based on 'diffraction theory' [2, 6 - 8], according to which sound is produced when the hydrodynamic pressure field of turbulence is swept over the edge in the mean flow and diffracted by the edge, or on Lighthill's acoustic analogy theory used in conjunction with a *compact* Green's function tailored to the trailing edge geometry [2, 9 - 11]. These methods are equivalent at low Mach numbers; their advantage is that they unambiguously identify fluid-structure interactions at the trailing edge as the source of sound, as opposed to locations on the extensive, near planar airfoil surface upstream of the edge, where a numerical simulation of the predominantly incompressible flow would supply no information about source phasing. In other words, as with the original application of Lighthill's theory to free field turbulence quadrupole sources, both of these theoretical approaches provide estimates of the edge noise from a knowledge of the *incompressible* characteristics of the flow near the edge.

Numerical predictions of trailing edge noise that are consistent with measurements have been made by Wang [12, 13] and Wang & Moin [14] by combining the results of direct numerical simulations of incompressible trailing edge flows with an integral representation of the sound involving the compact Green's function. These calculations have hitherto treated the acoustic problem in terms of the Green's function for a trailing edge modeled by a semi-infinite rigid plate [9], but the method of conformal transformation permits more general edge geometries to be considered, including airfoils of finite thickness [2, 5] and finite chord (Chapter 1).

An important special case arises for a trailing edge with a detached 'flap' [15 - 17] (or with the deployment of a leading edge 'slat' [18]). Noise is generated at the side-edges of part-span flaps and also within the spanwise slot between the airfoil and flap. At very low Mach numbers, typical of those encountered in underwater applications, a compact Green's function can be constructed for dealing with the production of sound by side-edge sources [19, 20]; *two-dimensional* analytical models of the influence of the slot between the deployed flap and the airfoil have been examined by Howe [21, 22] for simplified aeroacoustic distributions.

However, to derive reliable analytical predictions of the intensities of noise produced by general, three dimensional hydroacoustic source distributions in the slot it necessary that Green's function takes explicit account of the doubly-connected trailing edge geometry. The radiated sound can then be calculated from measurements or from numerical simulations of the unsteady hydrodynamic flow in the slot. In this chapter a formula is developed for the compact Green's function for a flap of large aspect ratio in the limit of small mean flow Mach number, when the chord of the flap is small compared to the acoustic wavelength. In the first instance this is done by modeling the airfoil by a semi-infinite rigid plate with a detached flap in the form of a rigid strip at a small angle of attack to the airfoil. The leading and trailing edges of the slot and the trailing edge of the flap are sources of sound whose relative importance can be estimated from the functional form of the Green's function. These conclusions can be extended to an airfoil and flap of finite thickness and rounded edge geometry, provided the slot width is large compared to the thickness of the flap near its leading edge. Similarly, a correction can be introduced in the manner described in Chapter 1 to take account of the finite chord of the airfoil.

The general representation of sound produced at low Mach numbers by fluid-structure interactions is recalled in §2. The Green's function for a flap at small angle of attack is

derived in §3, and approximations are obtained for its behavior near the edges of the flap and airfoil. The radiation efficiencies of the different edges are discussed (§4), and leading edge, flap-impingement noise is identified as the most important source in the slot. It is shown for this case how the noise can be represented in terms of an equivalent dipole source (whose strength is equal to the unsteady lift on the flap) placed at a suitable position to the rear of the airfoil.

2.2. FORMULATION OF THE PROBLEM

2.2.1 Trailing edge noise

Consider the generation of sound at low Mach numbers by turbulent flow in the vicinity of the trailing edge of an airfoil. It is first assumed that the trailing edge region has the idealized form illustrated in Figure 1. The airfoil is at rest within a mean stream at speed U in the positive x_1-direction of the rectangular coordinate system (x_1, x_2, x_3), and is modeled by a semi-infinite rigid plate occupying the half-plane $x_1 < 0,\ x_2 = 0$; the detached 'flap' consists of a uniform, rigid strip of width ℓ inclined at angle α to the airfoil. The slot separating the airfoil and the leading edge of the flap has width h. The objective is to determine the influence of the flap and slot on the generation of aerodynamic sound, but no account will be taken of the side-edges of part span flaps.

Let $\mathbf{v}$ and $\boldsymbol{\Omega} = \text{curl}\,\mathbf{v}$ respectively denote the velocity and vorticity, and let c_0 be the speed of sound. When the mean flow Mach number $M = U/c_0 \ll 1$ (so that the convection of sound by the mean flow may be neglected), the acoustic pressure $p(\mathbf{x}, t) = \int_{-\infty}^{\infty} p(\mathbf{x}, \omega)\mathrm{e}^{-i\omega t}d\omega$ in the far field at position $\mathbf{x}$ and time t is given formally by [2, 5]

$$\frac{p(\mathbf{x},\omega)}{\rho_0} = \int \frac{\partial G}{\partial \mathbf{y}}(\mathbf{x},\mathbf{y},\omega)\cdot\big(\boldsymbol{\Omega}\wedge\mathbf{v}\big)(\mathbf{y},\omega)d^3\mathbf{y} - \nu\oint_S \boldsymbol{\Omega}(\mathbf{y},\omega)\wedge\frac{\partial G}{\partial \mathbf{y}}(\mathbf{x},\mathbf{y},\omega)\cdot\mathbf{n}\,dS(\mathbf{y}), \quad |\mathbf{x}|\to\infty, \tag{28}$$

where ρ_0 is the mean fluid density and ν is the kinematic viscosity. The second integral is over the airfoil surface S (with unit normal $\mathbf{n}$ directed *into* the fluid), and can be ignored when the Reynolds number is very large. $G(\mathbf{x}, \mathbf{y}, \omega)$ is the *time harmonic* acoustic Green's function, which satisfies

$$(\nabla^2 + \kappa_0^2)G = \delta(\mathbf{x} - \mathbf{y}), \quad \kappa_0 = \frac{\omega}{c_0}, \tag{29}$$

and has vanishing normal derivative $\partial G(\mathbf{x}, \mathbf{y}; \omega)/\partial y_n = 0$ on S. When $M \ll 1$ the acoustic pressure is determined to an excellent approximation by equation (1) by approximating $\mathbf{v}$ and $\boldsymbol{\Omega}$ in the integrands by their values for incompressible flow.

The sound can also be represented entirely as a surface integral over S by introducing the upwash velocity $\mathbf{v}_I$, defined by the Biot-Savart formula [23, 24]

$$\mathbf{v}_I(\mathbf{x}, t) = \text{curl}\int_{V_\delta} \frac{\boldsymbol{\Omega}(\mathbf{y}, t)d^3\mathbf{y}}{4\pi|\mathbf{x} - \mathbf{y}|}, \tag{30}$$

where the integration is confined to the nonlinear region V_δ of the hydrodynamic flow *outside* the viscous sublayers on S [5]. In this case

$$\frac{p(\mathbf{x},\omega)}{\rho_o} = \oint_S \left(G(\mathbf{x},\mathbf{y},\omega)\frac{\partial \mathbf{v}_I}{\partial t}(\mathbf{y},\omega) - \nu\boldsymbol{\Omega}(\mathbf{y},\omega)\wedge\frac{\partial G}{\partial \mathbf{y}}(\mathbf{x},\mathbf{y},\omega)\right)\cdot\mathbf{n}\,dS(\mathbf{y}), \quad |\mathbf{x}|\to\infty, \quad (31)$$

To use this formula a preliminary calculation would need to be performed to determine the unsteady vorticity distribution $\boldsymbol{\Omega}$ close to the airfoil. The velocity $\mathbf{v}_I$ is then calculated from equation (3); it is precisely the 'kinematic' velocity induced by the vortex field $\boldsymbol{\Omega}$ when the influence of 'image' vortices within S (i.e. the influence of *scattering* by S) is ignored.

Equations (1) and (4) give alternative, but equivalent representations of the sound in terms of the same Green's function $G(\mathbf{x},\mathbf{y},\omega)$ that has vanishing normal derivative on S. The choice of which formulation to use will in practice depend on the details of the problem at hand.

2.2.2 Acoustically compact flap

Trailing edge interaction noise is determined by the contributions to the integrals in (1) from the neighborhood of the edge region. The wavelength of the sound $\sim \delta/M$, where δ is the turbulence eddy length scale near the edge. The acoustic wavelength ($\sim 1/\kappa_o$) will therefore be much larger than the flap chord ℓ when $M \ll 1$, and the unsteady flow structures that generate edge noise are then very much closer than an acoustic wavelength from the trailing edge region. This means that the nondimensional source distance $\kappa_o\sqrt{y_1^2+y_2^2} \ll 1$, and Green's function may accordingly be expanded in powers of this parameter. The leading terms in the expansion when the observation point $\mathbf{x}$ lies in the acoustic far field are [2]

$$G(\mathbf{x},\mathbf{y},\omega) = G_0(\mathbf{x},\mathbf{y},\omega) + G_1(\mathbf{x},\mathbf{y},\omega) + \ldots, \quad |\mathbf{x}-y_3\mathbf{i}_3|\to\infty, \quad (32)$$

where $\mathbf{i}_3$ is a unit vector in the spanwise (x_3-) direction, and

$$G_0(\mathbf{x},\mathbf{y},\omega) = \frac{-e^{i\kappa_o|\mathbf{x}-y_3\mathbf{i}_3|}}{4\pi|\mathbf{x}-y_3\mathbf{i}_3|}, \quad G_1(\mathbf{x},\mathbf{y},\omega) = \frac{-\sqrt{\kappa_o}\sin^{\frac{1}{2}}\psi\sin\left(\frac{\theta}{2}\right)\varphi^*(\mathbf{y})e^{i\kappa_o|\mathbf{x}-y_3\mathbf{i}_3|}}{\pi\sqrt{2\pi i}|\mathbf{x}-y_3\mathbf{i}_3|}. \quad (33)$$

If $r=\sqrt{x_1^2+x_2^2}$, the shortest distance of $\mathbf{x}$ from the edge of the airfoil (the x_3-axis), then $\psi = \sin^{-1}(r/|\mathbf{x}|)$ is the angle shown in Figure 1 between the direction of $\mathbf{x}$ and the edge, and (r,θ) are the polar coordinates of $\mathbf{x}$ in a plane x_3 = constant, so that

$(x_1, x_2) = r(\cos\theta, \sin\theta)$. The function $\varphi^*(\mathbf{y}) \equiv \varphi^*(y_1, y_2)$ of the source position $\mathbf{y}$ satisfies Laplace's equation, and has the simple interpretation as a velocity potential of ideal, incompressible flow in the anticlockwise direction in the figure around the edge, with zero circulation about the flap. It is normalized by the requirement that

$$\varphi^*(\mathbf{y}) \to \varphi_o^*(\mathbf{y}) \equiv \sqrt{r'}\sin(\theta'/2), \quad \text{as} \quad r' \to \infty, \quad \text{where } (y_1, y_2) = r'(\cos\theta', \sin\theta'), \tag{34}$$

where $\varphi_o^*(\mathbf{y})$ is the velocity potential of flow around the rigid *half-plane* $x_1 < 0,\ x_2 = 0$ [23, 24].

The zeroth order component G_0 in the expansion (5) has the same structure as the free space acoustic Green's function, and when used in (1) or (4) yields contributions to the acoustic pressure that are equivalent to the sound generated by free field turbulence *quadrupoles*. The main contribution to the radiation (whose amplitude is larger by a factor $\sim 1/M^{\frac{3}{2}} \gg 1$ than that produced by the quadrupoles) is generated by 'edge scattering' and is governed in a first approximation by the second term G_1 in equation (5). In the high Reynolds number limit, when surface shear stresses are small relative to the normal surface stresses, equations (1) and (4) therefore yield the following alternative, leading order representations

$$\begin{aligned} p(\mathbf{x},\omega) &\approx \frac{-\rho_o \kappa_o^{\frac{1}{2}} \sin^{\frac{1}{2}}\psi \sin(\theta/2)}{\pi\sqrt{2\pi i}|\mathbf{x}|} \int \frac{\partial\varphi^*(\mathbf{y})}{\partial \mathbf{y}} \cdot \big(\mathbf{\Omega} \wedge \mathbf{v}\big)(\mathbf{y},\omega) \mathrm{e}^{i\kappa_o|\mathbf{x}-iy_3\mathbf{i}_3|} d^3\mathbf{y} \\ &= \frac{\rho_o \omega\sqrt{i\kappa_o}\sin^{\frac{1}{2}}\psi\sin(\theta/2)}{\pi\sqrt{2\pi}|\mathbf{x}|} \oint_S \varphi^*(\mathbf{y}) v_{In}(\mathbf{y},\omega)\mathrm{e}^{i\kappa_o|\mathbf{x}-iy_3\mathbf{i}_3|} d\mathrm{S}(\mathbf{y}), \quad |\mathbf{x}| \to \infty, \end{aligned} \tag{35}$$

where $v_{In} = \mathbf{v}_\mathrm{I} \cdot \mathbf{n}$ and $\partial\mathbf{v}_\mathrm{I}/\partial t$ in (4) has been replaced by $-i\omega\mathbf{v}_\mathrm{I}$.

2.3. GREEN'S FUNCTION

2.3.1 Calculation of φ^*

The function $\varphi^*(\mathbf{y}) \equiv \varphi^*(y_1, y_2)$ is equivalent to the velocity potential of two-dimensional, incompressible flow around the trailing edge region of the airfoil, and may be determined by the method of conformal transformation [23, 24]. In the thin plate approximation, the airfoil occupies the negative real axis in the plane of $z = y_1 + iy_2$; the flap lies along the ray $\arg z = -\alpha$ between $z = he^{-i\alpha}$ and $z = He^{-i\alpha}$, where $H = \ell + h$ (see Figure 2a).

The transformation

$$\zeta = \sqrt{\frac{z}{h}} \tag{36}$$

maps the fluid region bounded by the airfoil and flap onto the right half of the ζ-plane, with the 'upper' and 'lower' sides ($A_\infty O$ and $B_\infty O$ respectively) of the airfoil mapping onto the imaginary axis, as indicated in Figure 2b. The flap maps into the interval $\zeta = e^{-i\epsilon}$ to $\zeta = e^{-i\epsilon}/\sqrt{m}$ of the ray $\arg \zeta = -\epsilon$, where $\epsilon = \alpha/2$ and $m = h/H$.

Irrotational flow in the anticlockwise sense around the trailing edge region in the z-plane corresponds to flow past the flap in the ζ-plane from $\zeta = -i\infty$ to $\zeta = +i\infty$ that becomes parallel to the imaginary axis as $|\zeta| \to \infty$. We can write

$$\varphi^*(\mathbf{y}) = \mathrm{Re}\, w(\zeta), \tag{37}$$

where $w(\zeta)$ is the complex potential of the flow in the ζ-plane. The potential can be calculated in closed form when $\epsilon = \alpha/2 = 0$; the solution for $\epsilon \neq 0$ is found by iteration, by writing

$$w(\zeta) = w_0(\zeta) + \epsilon w_1(\zeta) + \cdots, \text{ i.e. } \varphi^*(\mathbf{y}) = \varphi_0^*(\mathbf{y}) + \epsilon\varphi_1^*(\mathbf{y}) + \cdots. \tag{38}$$

The zeroth order problem for $w_0(\zeta)$ is illustrated in Figure 2c. The flap lies along the real axis between $\zeta = 1,\ 1/\sqrt{m}$; the imaginary axis forms a rigid barrier that may be removed by introducing an image flap on the negative real axis. At large distances from the flap in the z-plane equation (7) requires that $w(z) \to -i\sqrt{z}$; in the ζ-plane the flow is uniform and parallel to the imaginary axis when $|\zeta|$ is large, and $w_0(\zeta) \to w(\zeta) \approx -i\sqrt{h}\zeta$.

The functional form of $w_0(\zeta)$ with this limiting behavior can be found by Sedov's method ([25], Chapter 2) to be given by

$$w_0(\zeta) = -i\sqrt{H}\int_0^\zeta \left(\sqrt{1-mt^2} - \frac{\beta}{\sqrt{1-mt^2}}\right)\frac{dt}{\sqrt{1-t^2}}, \quad \beta = \text{constant}. \tag{39}$$

The value of β is determined by the condition that the circulation about the flap should vanish, which yields

$$\beta = 1 - \frac{E(m')}{K(m')} > 0, \quad m' = 1 - m, \tag{40}$$

where $K(m')$, $E(m')$ are respectively complete elliptic integrals of the first and second kinds [26].

Higher order approximations to $w(\zeta)$ can be determined successively by imposing the condition $\mathbf{n} \cdot \nabla\varphi^* = 0$ on the flap. If $\zeta = \xi + i\eta$, then correct to $O(\epsilon)$ we must satisfy

$$\frac{\partial\varphi_1^*}{\partial\eta} = -\frac{\partial\varphi_0^*}{\partial\xi}, \quad \text{for } 1 < \xi < 1/\sqrt{m}, \quad \eta = 0. \tag{41}$$

It follows from the symmetry of the problem that $\partial\varphi_0^*/\partial\xi$ is an odd function of η, and therefore, from (14), that φ_1^* represents the field of a *monopole* source distributed over $1 < \xi < 1/\sqrt{m}$, $\eta = 0$. Accordingly, application of the method of images supplies the solution

$$w_1(\zeta) = \frac{-\sqrt{H}}{\pi} \int_1^{1/\sqrt{m}} \ln(t^2 - \zeta^2) \left(\sqrt{1 - mt^2} - \frac{\beta}{\sqrt{1 - mt^2}} \right) \frac{dt}{\sqrt{t^2 - 1}}, \tag{42}$$

which has zero circulation about the flap.

A more convenient representation is obtained by considering the corresponding expression for $dw_1/d\zeta$, obtained by differentiation of (15). The integral can be transformed into an integral around a closed contour in the ζ-plane that just encloses the segment $(1,\ 1/\sqrt{m})$ of the real axis. Cauchy's theorem permits the integral to be replaced by one along the imaginary axis together with a contribution from a simple pole at $t = \zeta$ (in $\mathrm{Re}\,\zeta > 0$), i.e.

$$\begin{aligned} \frac{dw_1}{d\zeta} &= \frac{2\zeta\sqrt{H}}{\pi} \int_1^{1/\sqrt{m}} \frac{(1 - \beta - mt^2)}{\sqrt{t^2 - 1}\sqrt{1 - mt^2}} \frac{dt}{(t^2 - \zeta^2)} \\ &\equiv \frac{\sqrt{H}(1 - \beta - m\zeta^2)}{\sqrt{1 - \zeta^2}\sqrt{1 - m\zeta^2}} - \frac{\zeta\sqrt{H}}{\pi} \int_{-\infty}^{\infty} \frac{(1 - \beta + m\lambda^2)}{\sqrt{1 + \lambda^2}\sqrt{1 + m\lambda^2}} \frac{d\lambda}{(\lambda^2 + \zeta^2)}. \end{aligned} \tag{43}$$

Hence, using this and equation (12), we find

$$\begin{aligned} \frac{dw}{dz} &\equiv \frac{\partial\varphi^*}{\partial y_1} - i\frac{\partial\varphi^*}{\partial y_2} \approx \frac{dw_0}{dz} + \epsilon\frac{dw_1}{dz} \\ &= \frac{-i[z - (1 - \beta)H]}{2\sqrt{z}\sqrt{z - h}\sqrt{z - H}} \left(1 + \frac{i\alpha}{2}\right) - \frac{\alpha}{4\pi} \int_{-\infty}^{\infty} \frac{[\mu^2 + (1 - \beta)H]}{\sqrt{H + \mu^2}\sqrt{h + \mu^2}} \frac{d\mu}{(\mu^2 + z)}. \end{aligned} \tag{44}$$

The real and imaginary parts of this formula determine the functional form of $\partial\varphi^*(\mathbf{y})/\partial\mathbf{y}$, which may be used in the first of equations (8) to evaluate the edge noise when the vorticity and velocity distributions, $\mathbf{\Omega}$ and $\mathbf{v}$, are known near the flap (c.f. [13, 14]).

To calculate the sound using the second of equations (8), note first that for a thin airfoil it can be written in the form

$$p(\mathbf{x},\omega) \approx \frac{\rho_0\omega\sqrt{i\kappa_0}\sin^{\frac{1}{2}}\psi\sin(\theta/2)}{\pi\sqrt{2\pi}|\mathbf{x}|}\int_{S_+}\left[\varphi^*(\mathbf{y})\right]v_{In}(\mathbf{y},\omega)e^{i\kappa_0|\mathbf{x}-iy_3\mathbf{i}_3|}dS(\mathbf{y}), \quad |\mathbf{x}|\to\infty, \quad (45)$$

where the integration is over the 'upper' surfaces S_+ of the airfoil and flap, and $[\varphi^*] = \varphi^*_+ - \varphi^*_-$ is the jump in the value of φ^* in passing from the point $\mathbf{y}$ on the lower surface to the corresponding point on the upper surface. We can determine $[\varphi^*]$ by integrating the jump $d[w]/dz$ defined by equation (17). Introducing the approximation $1 + i\alpha/2 \approx e^{\frac{i\alpha}{2}}$, we find

$$\begin{aligned}\left[\varphi^*\right] &= 2\sqrt{\frac{|y_1|(H-y_1)}{h-y_1}} - 2H^{\frac{1}{2}}\left\{\mathcal{E}\left(\tan^{-1}\left(\sqrt{|y_1|/h}\right),m'\right)\right. \\ &\left. -(1-\beta)\mathcal{F}\left(\tan^{-1}\left(\sqrt{|y_1|/h}\right),m'\right)\right\}, \quad y_1 < 0 \text{ on the airfoil,} \end{aligned} \quad (46)$$

$$\begin{aligned}\left[\varphi^*\right] &= 2\sqrt{\frac{(H-y_{||})(y_{||}-h)}{y_{||}}} - 2H^{\frac{1}{2}}\left\{\mathcal{E}\left(\sin^{-1}\left(\sqrt{H(y_{||}-h)/y_{||}\ell}\right),m'\right)\right. \\ &\left. -(1-\beta)\mathcal{F}\left(\sin^{-1}\left(\sqrt{H(y_{||}-h)/y_{||}\ell}\right),m'\right)\right\}, \quad h < y_{||} < H \text{ on the flap,} \end{aligned} \quad (47)$$

where

$$\mathcal{E}(\xi,m') = \int_0^\xi \sqrt{1-m'\sin^2\mu}\,d\mu, \quad \mathcal{F}(\xi,m') = \int_0^\xi \frac{d\mu}{\sqrt{1-m'\sin^2\mu}}, \quad (48)$$

and $y_{||}$ denotes distance measured parallel to the surface of the flap (i.e., in a direction inclined at the flap angle α) from the edge O of the airfoil.

2.3.2 Critical behavior near the edges of the flap and airfoil

The solid curves in Figure 3 represent the potential flow streamlines $\psi_0^* =$ constant for the zeroth approximation $w_0 = \varphi_0^* + i\psi_0^*$ when $\ell = 4h$ ($m = 0.2$), calculated from equation (12) by setting $\zeta = \sqrt{zh}$. The volume flux between neighboring streamlines is the same in all cases; thus convergence of the streamlines near the leading and trailing edges of

the slot between the airfoil and flap, and near the trailing edge of the flap correspond to regions where $\nabla\varphi_0^*$ is large and where, according to equation (8), the efficiency of edge scattering of turbulence sources becomes large. The stagnation streamline intersects the flap symmetrically and corresponds to the broken line curve in the figure.

The behaviors of $\varphi^*(\mathbf{y}) \equiv \mathrm{Re}\, w(\zeta)$ near the edges of the flap and airfoil are determined by expanding $w(\zeta) \equiv w(\sqrt{z/h})$ about the critical points at $z = 0,\ h,\ H\ (= \ell + h)$. To the present order-$\epsilon$ approximation, the singularities at $z = 0,\ h$, and H occur respectively at the edge of the airfoil, and at the leading and trailing edges of the flap. By expanding the second line of (17) about each of these points and integrating with respect to z we find (after discarding irrelevant constants of integration)

$$\begin{aligned}
&\text{airfoil trailing edge:} \quad w \sim -i\sqrt{z}(1-\beta)\sqrt{1+\tfrac{\ell}{h}} \\
&\text{flap leading edge:} \quad w \sim \sqrt{z-h}\,\mathrm{e}^{\frac{i\alpha}{2}}\left[(1-\beta)\left(1+\tfrac{\ell}{h}\right)-1\right]\sqrt{\tfrac{h}{\ell}} \\
&\text{flap trailing edge:} \quad w \sim -i\sqrt{z-(h+\ell)}\,\mathrm{e}^{\frac{i\alpha}{2}}\beta\sqrt{1+\tfrac{h}{\ell}}.
\end{aligned} \tag{49}$$

The corresponding approximations for $\varphi^*(\mathbf{y}) = \mathrm{Re}\, w$ can be written

$$\begin{aligned}
&\text{airfoil trailing edge:} \quad \varphi^* \sim \sqrt{r_O}\sin\left(\tfrac{\theta_O}{2}\right)(1-\beta)\sqrt{1+\tfrac{\ell}{h}} \\
&\text{flap leading edge:} \quad \varphi^* \sim \sqrt{r_h}\cos\left(\tfrac{\theta_h+\alpha}{2}\right)\left[(1-\beta)\left(1+\tfrac{\ell}{h}\right)-1\right]\sqrt{\tfrac{h}{\ell}} \\
&\text{flap trailing edge:} \quad \varphi^* \sim \sqrt{r_H}\sin\left(\tfrac{\theta_H+\alpha}{2}\right)\beta\sqrt{1+\tfrac{h}{\ell}}
\end{aligned} \tag{50}$$

where (r_O, θ_O), (r_h, θ_h), (r_H, θ_H) are respectively the polar coordinates of the source point (y_1, y_2) relative to the edge O of the airfoil, to the flap leading edge, and the flap trailing edge.

2.4. TRAILING EDGE AND FLAP GENERATED SOUND

2.4.1 Trailing edge noise

An important component of the sound generated by the trailing edge region can be attributed to turbulence whose characteristic length scale is small compared to the flap chord ℓ. In this case the effective acoustic sources at the edges labelled O, A and B in Figure 4a will be statistically independent, and their relative contributions to the far field sound can be estimated by inserting the corresponding approximations (23) for $\varphi^*(\mathbf{y})$ into the second of equations (8) and performing local surface integrations.

The upwash velocity $\mathbf{v}_\mathrm{I}$ is produced by the turbulence convecting past the edges, augmented by the induced velocity of any additional vorticity shed from the trailing edges (to satisfy the unsteady *Kutta condition* [27]). The effect of this shedding is greatly to reduce the importance of the edges O and B as sources of sound, because the induced velocity of the shed vorticity acts to oppose that produced by impinging turbulence. This does not occur at the leading edge A: provided the flow does not separate near A, any vorticity generated there is swept downstream over the surface of the flap, and its induced velocity is therefore cancelled by an equal and opposite velocity produced by image vortices in the flap. Thus, impingement noise generated at A is likely to be the principal source of sound in the trailing edge region.

However, it is possible for the trailing edges O and B to remain significant sources of *high frequency* sound. It follows from equation (8) and by inspection of (23) that the relative *intensities* of the corresponding acoustic pressures p_O, p_B, say, is given by

$$\left(\frac{p_\mathrm{O}}{p_\mathrm{B}}\right)^2 \sim \left(\frac{v_O}{v_B}\right)^2 \frac{\ell}{h}\frac{(1-\beta)^2}{\beta^2}, \tag{51}$$

where v_O, v_B are characteristic turbulence velocities (e.g. friction velocities) respectively near the trailing edges of the airfoil and flap. The relative *efficiency* factor $10 \times \log_{10}[(\ell/h)(1-\beta)^2/\beta^2]$ (dB) determines the ratio of the intensities of the sound produced at O and B when the magnitudes of the turbulence velocities are nominally equal; it is plotted as a function of ℓ/h in Figure 5, from which it is seen that the efficiency of edge noise production at the trailing edge O of the airfoil exceeds that at the trailing edge of the flap typically by 7 dB or more.

2.4.2 Equivalent flap-impingement-noise dipole

Equations (8) and the second of (23) show that the acoustic pressure generated by small scale turbulence impinging on the leading edge of the flap at A is given by

$$p(\mathbf{x},\omega) \sim \frac{f\rho_0\omega\sqrt{2i\kappa_0}\sin^{\frac{1}{2}}\psi\sin(\theta/2)\mathrm{e}^{i\kappa_0|\mathbf{x}|}}{\pi^{\frac{3}{2}}|\mathbf{x}|}\int_{-\infty}^{\infty}dy_3\int_h^{\ell+h}\sqrt{y_{||}-h}\,v_\perp(y_{||},y_3,\omega)\mathrm{e}^{-i\kappa_0\cos\psi y_3}dy_{||},$$

$$|\mathbf{x}|\to\infty, \tag{52}$$

where $v_\perp(y_{||},y_3,\omega)$ is the normal component of the upwash velocity (directed 'upwards' from the flap), expressed in terms of the distance $y_{||}$ measured along the flap from A, and

$$f\equiv f\left(\frac{\ell}{h}\right)=\sqrt{\frac{h}{\ell}}\left[(1-\beta)\left(1+\frac{\ell}{h}\right)-1\right]. \tag{53}$$

The turbulence impinging on the leading edge A produces lift fluctuations on the flap. The magnitude of this lift force will be influenced to some extent by the proximity of the airfoil, but for small scale turbulence the influence will be small, and the force will be close to its value when the airfoil is absent. The lift per unit span at frequency ω for a thin-plate flap, when the reduced frequency $\omega\ell/U>1$, and when the influence of the main airfoil is ignored, is given by [2, 28]

$$F(y_3,\omega)=-2i\rho_0\omega\sqrt{\ell}\int_h^{\ell+h}\sqrt{y_{||}-h}\,v_\perp(y_{||},y_3,\omega)dy_{||}. \tag{54}$$

This is equivalent to the classical Sears formula [29] when $v_\perp(y_{||},y_3,\omega)$ is assumed *not* to depend on the spanwise coordinate y_3

Let us determine the sound generated by this force when it is assumed to be distributed along a spanwise line at distance ℓ_F to the rear of the airfoil *in the absence of a flap* (see Figure 6). The force on the fluid is $(0,-F,0)$ and the acoustic pressure is therefore determined by [2]

$$(\nabla^2+\kappa_0^2)p=-\frac{\partial}{\partial x_2}\Big(\delta(x_1-\ell_F)\delta(x_2)F(x_3,\omega)\Big), \tag{55}$$

subject to $\partial p/\partial x_2=0$ on the airfoil. The solution can be expressed in terms of the component $G_1(\mathbf{x},\mathbf{y},\omega)$ of Green's function (5), where $\varphi^*(\mathbf{y})$ is given by (7) in the absence of the flap:

$$p(\mathbf{x},\omega) = -\int G_1(\mathbf{x},\mathbf{y},\omega)\frac{\partial}{\partial y_2}\big(\delta(y_1-\ell_F)\delta(y_2)F(y_3,\omega)\big)d^3\mathbf{y}$$
$$= \frac{-\sqrt{\kappa_0}\sin^{\frac{1}{2}}\psi\sin(\theta/2)e^{i\kappa_0|\mathbf{x}|}}{2\pi\sqrt{2\pi i\ell_F}|\mathbf{x}|}\int_{-\infty}^{\infty}F(y_3,\omega)e^{-i\kappa_0\cos\psi y_3}dy_3$$
$$= \sqrt{\frac{\ell}{4\ell_F}}\frac{\rho_0\omega\sqrt{2i\kappa_0}\sin^{\frac{1}{2}}\psi\sin(\theta/2)e^{i\kappa_0|\mathbf{x}|}}{\pi^{\frac{3}{2}}|\mathbf{x}|}$$
$$\times\int_{-\infty}^{\infty}dy_3\int_h^{\ell+h}\sqrt{y_{\|}-h}\,v_\perp(y_{\|},y_3,\omega)e^{-i\kappa_0\cos\psi y_3}dy_{\|},\quad |\mathbf{x}|\to\infty. \tag{56}$$

This will coincide with the directly calculated radiation (24) if $\ell_F = \ell/4f^2$. In other words, provided the dipole F is situated downstream of the airfoil trailing edge O *when the presence of the flap is ignored* at a distance

$$\frac{\ell_F}{h} = \frac{(\ell/h)^2}{4\left[(1-\beta)\left(1+\frac{\ell}{h}\right)-1\right]^2}. \tag{57}$$

This function is plotted in Figure 6. Evidently ℓ_F/h increases very slowly as the chord of the flap increases (ultimately proportional to $[\ln(16\ell/h)/4]^2$), and ℓ_F does not exceed twice the slot width h until $\ell/h > 12$.

When the the statistical properties of $F(y_3,\omega)$ are known the frequency spectrum $\Phi(\mathbf{x},\omega)$ of the acoustic pressure at $\mathbf{x}$ (which satisfies $\langle p^2(\mathbf{x},t)\rangle = \int_{-\infty}^{\infty}\Phi(\mathbf{x},\omega)d\omega$, where $\langle\ \rangle$ denotes an ensemble average) is readily calculated. For stationary random turbulence

$$\langle F(y_3,\omega)F^*(y_3',\omega')\rangle = \delta(\omega-\omega')\Phi_{FF}(\omega)\mathcal{R}(|y_3-y_3'|,\omega), \tag{58}$$

where $\Phi_{FF}(\omega)$ is the frequency spectrum of the lift per unit span (defined such that $\langle|F(y_3,\omega)|^2\rangle = \int_{-\infty}^{\infty}\Phi_{FF}(\omega)d\omega$), and $\mathcal{R}(y,\omega)$ is the corresponding spanwise covariance (for which $\mathcal{R}(0,\omega)=1$).

In terms of these definitions, it is easily deduced from the second of equations (29) that

$$\Phi(\mathbf{x},\omega) \approx \frac{\sin\psi\sin^2(\theta/2)}{(2\pi)^3|\mathbf{x}|^2}\frac{L\ell_3}{c_0\ell_F}\omega\Phi_{FF}(\omega),\quad |\mathbf{x}|\to\infty, \tag{59}$$

where $\ell_3 = \int_0^{\infty}\mathcal{R}(y,\omega)dy$ is the spanwise correlation length of the lift and $L \gg \ell_3$ is the span of the flap wetted by the turbulent flow. The spanwise correlation scale is frequency dependent, and typically $\ell_3 \sim U/\omega$, so that $\kappa_0\ell_3 \sim M \ll 1$; this condition has been used in deriving (32). The order of magnitude of the flap mean square acoustic pressure is

$$\langle p^2\rangle \sim \left(\frac{\ell}{|\mathbf{x}|}\right)^2\left(\frac{L}{\ell_F}\right)(\rho_0U^2)^2M, \tag{60}$$

which is characteristic of edge generated sound when the airfoil chord is large compared to the acoustic wavelength.

2.4.3 Airfoil and flap of finite thickness

These detailed conclusions are applicable to the more general trailing edge configuration sketched in Figure 4b. The formulae (23) for $\varphi^*(\mathbf{y})$ now constitute 'outer approximations' to the potential function defining irrotational flow around the trailing edge region. $\varphi^*(\mathbf{y})$ varies in a more complicated manner close to the rounded edges of the flap, or near the thickened geometry of the airfoil trailing edge, but will tend to the forms given in (23) when the distance from an edge exceeds the edge radius of curvature. This indicates that the above predictions of, say, the flap impingement noise should still be valid for components of the upwash velocity whose length scales are larger than the leading edge radius of curvature of the flap. But these would be expected to be the dominant small scale noise sources, since the efficiency of sound generation tends to fall off rapidly when the turbulence scale becomes smaller than the radius of curvature [2]. In particular the result in Figure 6 for the location of the effective flap dipole source should remain true for the dominant turbulence sources.

2.5. CONCLUSION

The sound produced by a trailing edge flap with a detached flap has three principal sources. First there is the 'self noise' attributed to small scale turbulence produced by instabilities in the boundary layers upstream of the airfoil and flap trailing edges. This is of relatively high frequency, because the sound that would be generated by larger scale turbulence eddies (large on a scale of airfoil or flap thickness near the edge) tends to be cancelled by that produced by vorticity shed from the edge in accordance with the Kutta condition. Second, impingement noise is produced when turbulence is swept past the leading edge of the flap, creating an unsteady lift force that generates sound by interaction with the trailing edge of the airfoil. Finally, the side edges of part-span flaps constitute an important source of lower frequency noise, associated with the interaction of side-edge lift vortices with the side-edge and trailing edge.

The formulae given in this chapter for the compact Green's function for a trailing edge with a single detached flap can be used to estimate the trailing edge self-noise and the flap impingement noise in flows at low Mach number. The analytical results for a flap at a modest angle of attack α (where $\alpha^2 \ll 1$) indicate that the self-noise produced at the edge of the airfoil is typically at least 7dB in excess of that produced at the flap trailing edge. The strength of the noise generated by impingement on the flap leading edge can be calculated by first determining the unsteady lift $F(\omega)$ per unit span produced by the turbulence when the flap is regarded as an *isolated airfoil*, for example, by means of a convenient 'strip-theory' approximation based on Sears' formula for the lift produced by a gust. The radiation is then equal to that produced by a dipole of strength $-F$ situated at distance ℓ_F to the rear of the edge of the main airfoil; this distance is given as a function of flap dimensions by equation (26). The dipole radiation intensity is increased from its classical free field value by the proximity of the airfoil trailing edge, typically by a factor $\sim \mathrm{O}(1/M)$ $(\gg 1)$; similarly its directivity is modified by the presence of the airfoil.

In this chapter it has been assumed that the airfoil chord is much larger than all other length scales, including the acoustic wavelength. This condition can be relaxed, however (provided the characteristic acoustic wavelength remains large compared to the flap chord), without changing the principal conclusions, by introducing the frequency-dependent correction factor given in Chapter 1 for dealing with airfoils of finite chord. Predictions of this chapter can therefore be used to validate acoustic numerical prediction schemes applied to a finite chord airfoil with a detached flap of suitably simple geometry.

REFERENCES

1. N. Curle 1955 *Proceedings of the Royal Society* **A231**, 505 -514. The influence of solid boundaries upon aerodynamic sound.
2. M. S. Howe 1998 *Acoustics of Fluid-Structure Interactions*, Cambridge University Press.
3. J. E. Ffowcs Williams and D. L. Hawkings 1969 *Philosophical Transactions of the Royal Society* **A264**, 321 -342. Sound generation by turbulence and surfaces in arbitrary motion.
4. J. C. Hardin and J. E. Martin 1997 *American Institute of Aeronautics and Astronautics Journal* **35**, 810 - 815. Flap side-edge noise: acoustic analysis of Sen's model.
5. M. S. Howe 1999 *Journal of Sound and Vibration* **225**, 211 - 238. Trailing edge noise at low Mach numbers
6. D. M. Chase 1972 *Journal of the Acoustical Society of America* **52**, 1011 - 1023. Sound radiated by turbulent flow off a rigid hal-plane as obtained from a wavevector spectrum of hydrodynamic pressure.
7. K. L. Chandiramani 1974 *Journal of the Acoustical Society of America* **55**, 19 - 29. Diffraction of evanescent waves, with applications to aerodynamically scattered sound and radiation from unbaffled plates.
8. D. M. Chase 1975 *American Institute of Aeronautics and Astronautics Journal* **13**, 1041 - 1047. Noise radiated from an edge in turbulent flow.
9. M. J. Lighthill 1952 *Proceedings of the Royal Society* **A211**, 564 - 587. On sound generated aerodynamically. Part I: General theory.
10. M. J. Lighthill 1954 *Proceedings of the Royal Society* **A222**, 1 - 32. On sound generated aerodynamically. Part II: Turbulence as a source of sound.
11. J. E. Ffowcs Williams and L. H. Hall 1970 *Journal of Fluid Mechanics* **40**, 657 - 670. Aerodynamic sound generation by turbulent flow in the vicinity of a scattering half-plane.
12. M. Wang 1997 *Annual Research Briefs* 37 - 49, (Center for Turbulence Research, Stanford University). Progress in large-eddy simulation of trailing-edge turbulence and aeroacoustics.

13. M. Wang 1998 *Annual Research Briefs* 91 -106, (Center for Turbulence Research, Stanford University). Computation of trailing-edge noise at low mach number using LES and acoustic analogy.

14. M. Wang and P. Moin 1999 Submitted to *A. I. A. A. J.* Computation of trailing-edge noise using large-eddy simulation.

15. T. Z. Dong, C. K. W Tam and N. N. Reddy 1999 *AIAA Paper* 99-1803. Direct numerical simulation of flap side edge noise.

16. T. H. Wood and S. M. Grace 1999 *AIAA Paper* 99-1893. Aeroacoustic predictions of a wing-flap configuration in three dimensions.

17. T. H. Wood and S. M. Grace 2000, *AIAA Paper* 0607. Free-wake analysis for calculating the aeroacoustics of a wing-flap configuration.

18. Y. P. Guo 1997 *AIAA Paper* 97-1647. A model for slat-noise generation.

19. M. S. Howe 1982 *Journal of Sound and Vibration* **80**, 555 - 573. On the generation of side-edge flap noise.

20. M. S. Howe 1998 *Reference manual on the theory of lifting surface noise at low Mach numbers.* Boston University, Department of Aerospace and Mechanical Engineering Report AM-98-001.

21. M. S. Howe 1978 *Aeronautical Research Council Reports & Memoranda No. 3830*: The generation of sound by a slot in an aerofoil.

22. M. S. Howe 1980 *Proceedings of the Royal Society* **A373**, 253 - 272. Aerodynamic sound generated by a slotted trailing edge.

23. Horace Lamb 1932 *Hydrodynamics* (6th. ed.). Cambridge University Press (Reprinted 1993).

24. G. K. Batchelor 1967 *An Introduction to Fluid Dynamics.* Cambridge University Press.

25. L. I. Sedov 1965 *Two Dimensional Problems in Hydrodynamics and Aerodynamics.* New York: John Wiley.

26. M. Abramowitz and I. A. Stegun (editors) 1970 *Handbook of Mathematical Functions* (ninth corrected printing), US Department of Commerce, National Bureau of Standards Applied Mathematics Series No.55.

27. D. G. Crighton 1985 *Annual Reviews of Fluid Mechanics* **17**, 411 - 445. The Kutta condition in unsteady flow.

28. M. S. Howe 1999 *J. Fluids and Structures* (submitted). Unsteady lift and sound produced by an airfoil in a turbulent boundary layer.

29. W. R. Sears 1941 *Journal of the Aeronautical Sciences* **8**, 104 - 108. Some aspects of non-stationary airfoil theory and its practical applications.

30. M. J. Lighthill 1958 *An introduction to Fourier analysis and generalised functions.* Cambridge University Press.

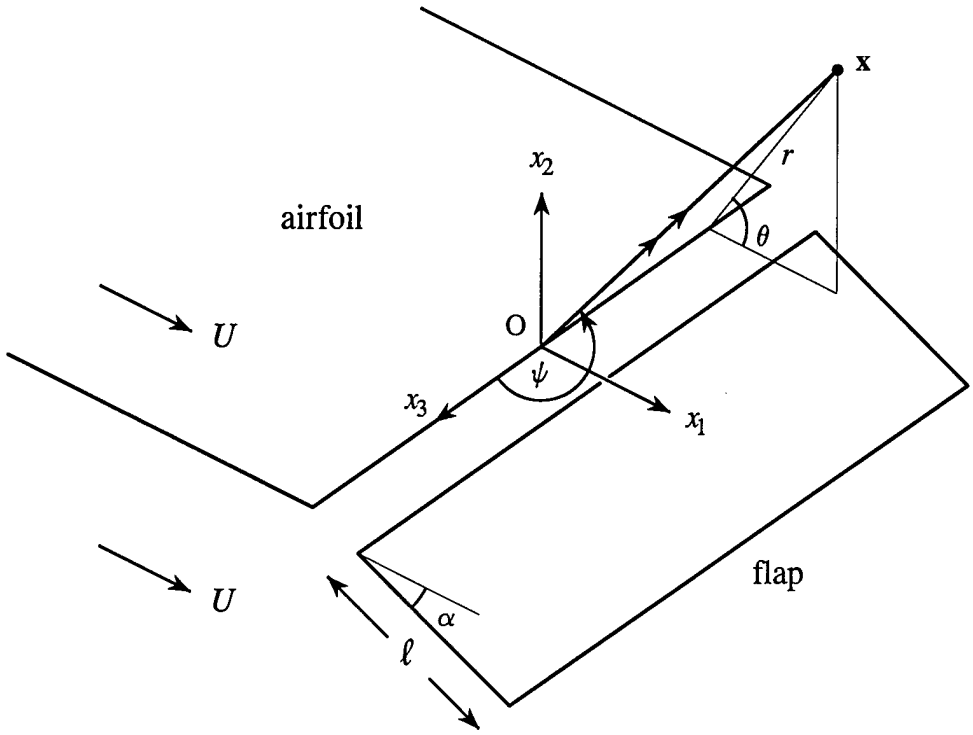

Figure 1. Idealized airfoil and flap, illustrating the angles θ and ψ defining the point $\mathbf{x}$ in the acoustic far field.

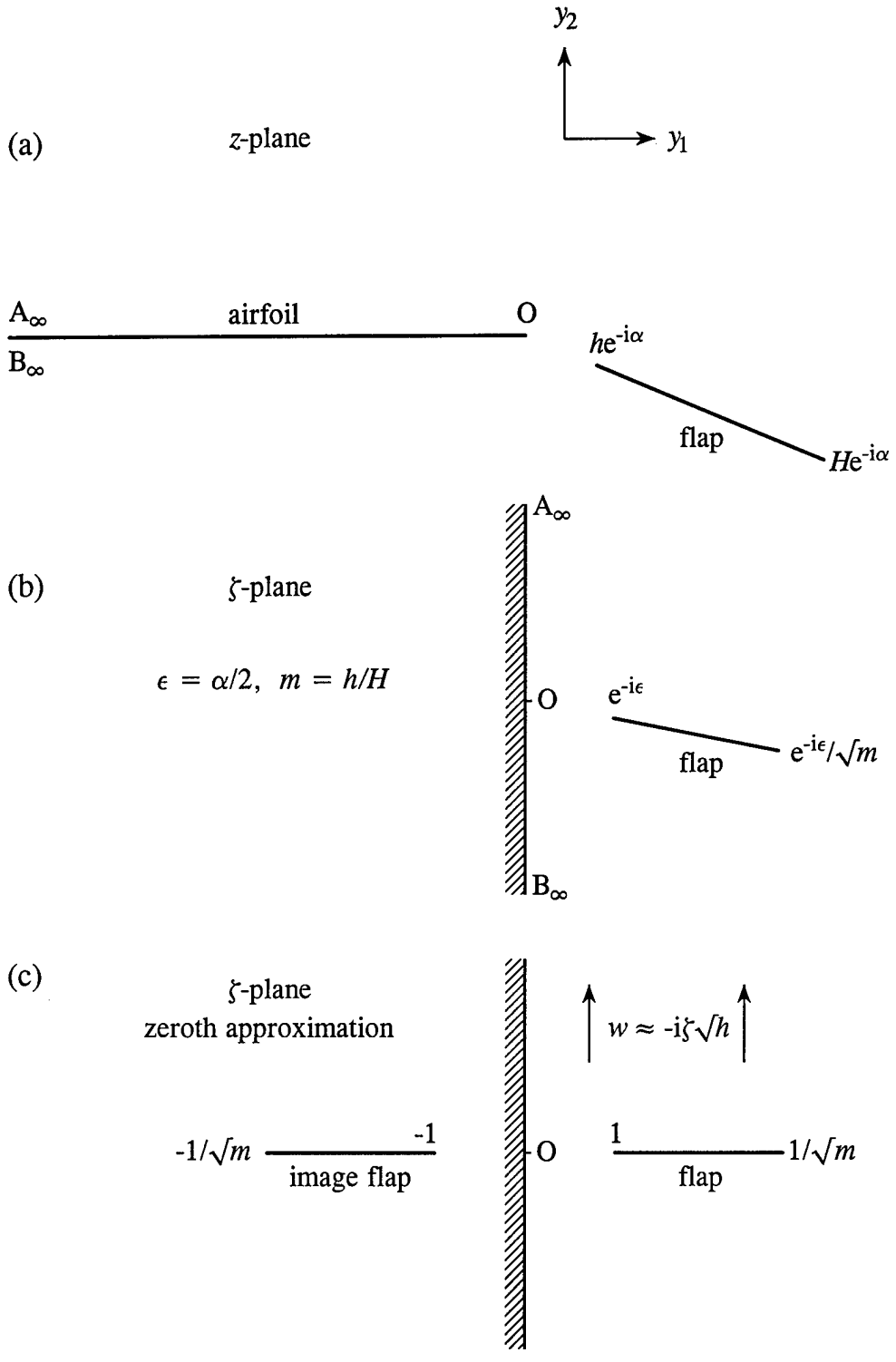

Figure 2. (a) Thin plate airfoil and flap in the z-plane; (b) Image in the ζ-plane; (c) Configuration in the ζ-plane in the zeroth approximation.

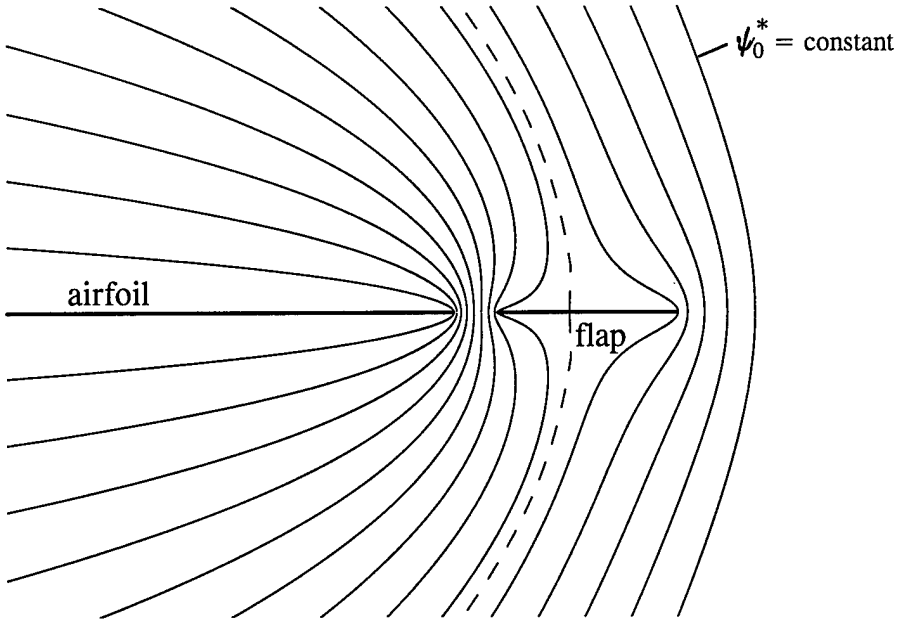

Figure 3. Streamlines $\psi_0^* =$ constant in the z-plane for the zeroth order approximation $w_0 = \varphi_0^* + i\psi_0^*$ when $\ell = 4h$.

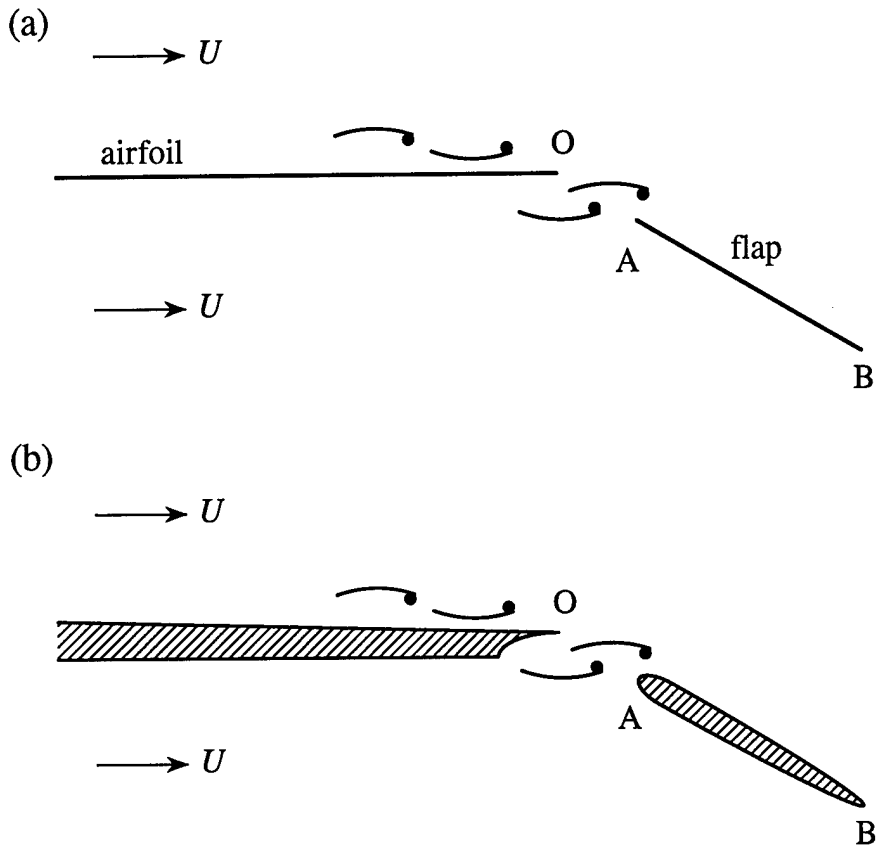

Figure 4. (a) Turbulence interacting with the airfoil and flap; (b) Generalized trailing edge configuration.

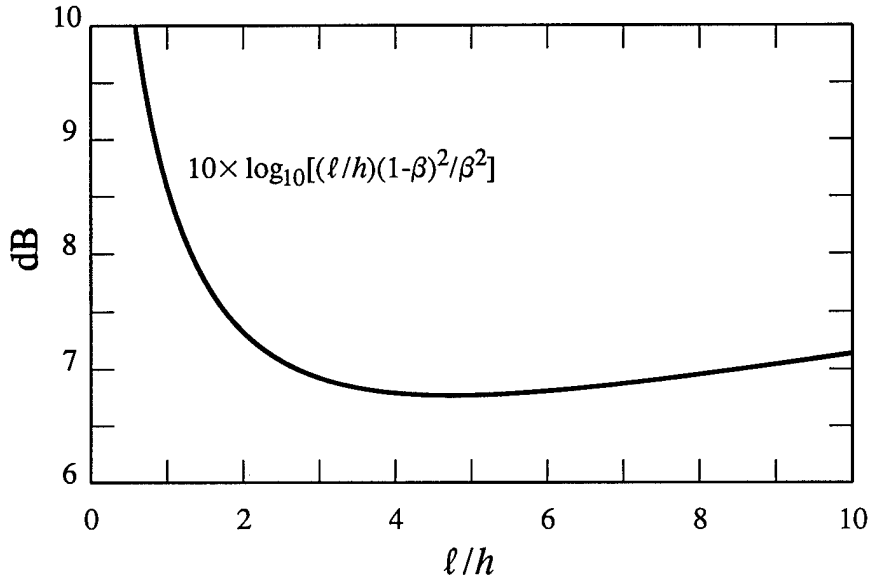

Figure 5. Relative efficiency of trailing edge noise generation at O and B in Figure 4.

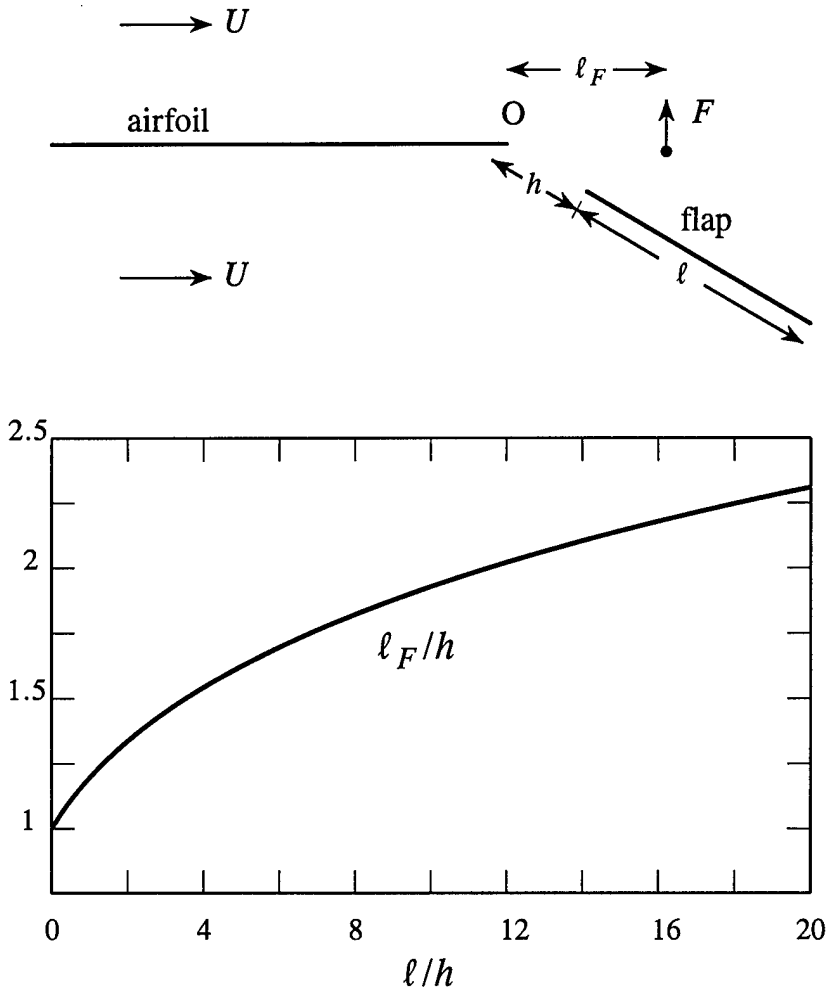

Figure 6. Line of action of equivalent dipole lift force F for calculating flap leading-edge-impingement noise.

REPORT DOCUMENTATION PAGE

Form Approved
OMB No. 0704-0188

1. AGENCY USE ONLY (Leave blank)	2. REPORT DATE	3. REPORT TYPE AND DATES COVERED
	27 March 2000	Final. 1 May 1999 - 31 Mar. 2000

4. TITLE AND SUBTITLE
Fluid-Structure Interaction Noise Predicted From Large Eddy Simulations

5. FUNDING NUMBERS
N00014-99-1-0391

6. AUTHOR(S)
Michael S. Howe

7. PERFORMING ORGANIZATION NAME(S) AND ADDRESS(ES)
Boston University
College of Engineering
110 Cummington Street
Boston MA 02215

8. PERFORMING ORGANIZATION REPORT NUMBER
AM-00-003

9. SPONSORING/MONITORING AGENCY NAME(S) AND ADDRESS(ES)
Office of Naval Research
Code 333
Dr. L. Patrick Purtell

10. SPONSORING/MONITORING AGENCY REPORT NUMBER

11. SUPPLEMENTARY NOTES

12a. DISTRIBUTION/AVAILABILITY STATEMENT
Approved for Public Release; distribution is unlimited

12b. DISTRIBUTION CODE

13. ABSTRACT *(Maximum 200 words)*

Approximations are derived for the three-dimensional Green's function for an airfoil of finite thickness and chord for sources near the leading or trailing edge. The acoustic wavelength is large relative to the airfoil thickness, but no restriction is placed on its magnitude relative to the chord. Extension is made to production of sound by flow over the trailing edge of an airfoil with a single detached flap. Green's function is derived for a detached flap at relative angle of attack α when the chord of the flap is acoustically compact. Formulae are given for calculating the `self-noise' produced by boundary layer instability; the efficiency of sound generation at the edge of the airfoil is shown to be typically at least 7dB larger than that produced at the trailing edge of the flap. The results can be incorporated into a numerical scheme for predicting airfoil noise at low Mach numbers.

14. SUBJECT TERMS
Aerodynamic sound, edge noise, vortex sound, trailing edge, thickness effects, flap

15. NUMBER OF PAGES
50 + i

16. PRICE CODE

17. SECURITY CLASSIFICATION OF REPORT	18. SECURITY CLASSIFICATION OF THIS PAGE	19. SECURITY CLASSIFICATION OF ABSTRACT	20. LIMITATION OF ABSTRACT
Unclassified	Unclassified	Unclassified	

ENGR (1)